SOT | Society of Toxicology
OXFORD
academic.oup.com/toxsci

Natural variation suggests candidate genes underlying *Caenorhabditis elegans* susceptibility to diverse toxicants

Timothy A. Crombie [1,‡], Ryan Mckeown [2,3,‡], Samuel J. Widmayer [2], Amanda O. Shaver [4], Nicolas D. Moya [4,5], J. B. Collins [4], Janneke Wit [2], Robyn E. Tanny [4], Christian Braendle [6], Lewis Stevens [7], Lisa Van Sluijs [8], Matthew V. Rockman [9], Mark G. Sterken [8], Marie-Anne Félix [10], Erik C. Andersen [4,*]

[1]Department of Biomedical Engineering and Science, Florida Institute of Technology, Melbourne, FL, 32901, United States
[2]Molecular Biosciences, Northwestern University, Evanston, IL, 60208, United States
[3]Interdisciplinary Biological Sciences Program, Northwestern University, Evanston, IL, 60208, United States
[4]Department of Biology, Johns Hopkins University, Baltimore, MD, 21218, United States
[5]Program in Cell, Molecular, Developmental Biology, and Biophysics, Johns Hopkins University, Baltimore, MD, 21218, United States
[6]Université Côte d'Azur, CNRS, Inserm, IBV, Nice, 06100, France
[7]Wellcome Sanger Institute, Tree of Life, Wellcome Genome Campus, Cambridge, CB10 1SA, United Kingdom
[8]Laboratory of Nematology, Wageningen University & Research, Wageningen, the Netherlands
[9]Department of Biology and Center for Genomics & Systems Biology, New York University, New York, NY, 10003, United States
[10]Institut de Biologie de l'École Normale Supérieure, CNRS, Paris, France

*Corresponding author: Department of Biology, Johns Hopkins University, 3400 North Charles St., Bascom UTL 383, Baltimore, MD 21218, United States.
Email: Erik.andersen@gmail.com

‡These authors contributed equally.

Abstract

Genetic differences among individuals shape how they respond to environmental toxicants, but the identification and validation of the genes responsible for this variation is difficult, particularly in humans. Consequently, our limited knowledge of the genes that influence susceptibility constrains our ability to accurately predict the risks posed by environmental toxicants. To identify genes underlying natural differences in toxicant susceptibilities, we measured the effects of 23 environmental toxicants on larval development across 195 genetically diverse *Caenorhabditis elegans* strains using a high-throughput imaging platform. We then combined these response data with whole-genome sequences to perform genome-wide association mappings, identifying 40 genomic regions where genetic variants are correlated with susceptibility differences. Many of these regions are enriched for genes involved in biological processes previously linked with toxicant responses, supporting the potential contributions of these genes to natural variation in susceptibility. Using biologically informed heuristics based on genomic context and functional annotation, we prioritized genes for follow-up experimentation and identified 94 candidate susceptibility genes, offering feasible targets for experimental validation that could ultimately inform toxicant risk prediction and regulatory assessment by linking genetic variation to differences in susceptibility.
Analysis of natural genetic variation among 195 wild C. elegans strains identified 94 candidate genes putatively linked to differences in susceptibility to 23 environmental toxicants. These findings can inform the discovery of conserved susceptibility genes and the development of biomarkers that improve chemical risk assessment by accounting for genetic differences among humans.

Keywords: *Caenorhabditis elegans*; genome-wide association studies (GWAS); environmental toxicants; xenobiotic response; risk assessment

It is estimated that more than 350,000 chemicals or chemical mixtures are registered for production and use globally, yet the risks that most of these chemicals pose to human health remain unknown (Wang et al. 2020). Accurately characterizing chemical toxicity in humans is challenging, prompting researchers to rely on data from toxicity assays using human cell lines or animal models to predict risk (Rusyn et al. 2010; Zeise et al. 2013; Chiu and Rusyn 2018; Rusyn et al. 2022). However, most of these assays are performed in a single genetic background, limiting the ability of researchers to observe variability in adverse responses to environmental chemicals found in natural populations (Rusyn et al. 2022). Consequently, the full spectrum of genetic and molecular mechanisms that contribute to differences in toxicant susceptibility

among genetically diverse individuals remain largely unknown (Zeise et al. 2013; Alam and Jones 2014; Chiu and Rusyn 2018; Rusyn et al. 2022). This critical knowledge gap hinders efforts to understand the genetic determinants of susceptibility, recognize at-risk individuals, and establish evidence-based regulatory limits for chemicals (Zeise et al. 2013; Chiu and Rusyn 2018; Rusyn et al. 2022; To et al. 2023). A key step in closing this gap is the identification of genes that influence toxicant susceptibility.

Genome-wide association studies (GWAS) are a powerful method to identify genes that contribute to differences in toxicant susceptibilities among individuals. In a GWAS, researchers test for statistical associations between genetic variants, typically single-nucleotide variants (SNVs), and variation in a phenotype, such as

response to a toxicant, across a population of genetically diverse individuals (Barton and Keightley 2002; Broekema et al. 2020). These "marker" variants are distributed throughout the genome and are used to scan for genomic regions statistically associated with population-wide differences in susceptibility. In many cases, the associated regions contain variants that impact genes or regulatory elements that can alter protein function, gene expression, or molecular pathways relevant to toxicity. However, because GWAS identifies statistical correlations rather than direct causal relationships, experimental validation is required to determine whether candidate genes in associated regions truly affect toxicant susceptibility.

Human GWAS have identified a limited number of candidate genes associated with toxicant susceptibility by using toxicant levels in blood or urine as the focal trait. The susceptibility genes uncovered typically encode drug-metabolizing enzymes (Pierce et al. 2012; Evans et al. 2013) or toxicant-interacting proteins such as cellular transporters and metalloenzymes (Ng et al. 2015; Wahlberg et al. 2018; Moksnes et al. 2024). However, identification and validation of candidate susceptibility genes in humans are heavily constrained by confounding variables and ethical restrictions, including age, sex, environmental heterogeneity, and the inability to edit genes in human subjects (Alam and Jones 2014). To overcome these challenges, genetically diverse human cell lines have been used to assay toxicity, revealing candidate genes involved in solute transport, membrane function, immune response, cell division, and DNA replication (Abdo et al. 2015; Abdo et al. 2015; Ford et al. 2022). Although these *in vitro* models offer valuable insights into the genetic determinants of susceptibility, they are unable to capture the full complexity of whole-organism toxicant responses. For example, cell lines do not express all genes relevant to toxicant responses and the complex interactions between tissues and organ systems are absent (Wheeler and Dolan 2012). Recent advances in organoid technologies partially overcome these limitations by more accurately modeling the structural and functional complexity of human tissues, but current organoid models still lack the genetic diversity required to study population-level variation in susceptibility (Rossi et al. 2018; Co et al. 2023). Because of the limitations of human experiments, animal models are indispensable for conducting GWAS aimed at identifying genetic factors that influence toxicant susceptibility at the whole-organism level.

Several genetically diverse animal populations have been used to identify genetic factors that contribute to differences in susceptibility among individuals (Rusyn et al. 2022). For example, studies using genetically diverse rodent populations have identified candidate susceptibility genes involved in xenobiotic metabolism (Church et al. 2014; Yoo et al. 2015; Nguyen et al. 2017; You et al. 2020), immune response (Harrill et al. 2009), chromatin structure (Koturbash et al. 2011), and tissue repair pathways (Harrill et al. 2012; Tsuchiya et al. 2012; Harrill et al. 2018). In addition, high costs and ethical concerns surrounding animal welfare are significant barriers in rodent-based studies (Akhtar 2015). To address these barriers, the U.S. Environmental Protection Agency (EPA) has outlined a strategic plan to advance new approach methodologies (NAMs), including *in silico*, *in chemico*, and *in vitro* technologies, to reduce reliance on traditional animal models in toxicant risk assessment (USEPA 2018; Schmeisser et al. 2023). Similarly, the National Institutes of Health (NIH) has emphasized NAMs, either alone or in combination with data from tractable animal models, to study disease. In this context, small model organisms provide an attractive non-mammalian alternative, providing higher throughput, reduced cost, and limited ethical concerns that can better keep pace with rapid chemical production. Moreover, genetically diverse populations of *Drosophila melanogaster* (Zhou et al. 2017; Everman and Macdonald 2024; Hanson et al. 2025), *Danio rerio* (Balik-Meisner et al. 2018; Thunga et al. 2022), and *Caenorhabditis elegans* (Vertino et al. 2011; Andersen et al. 2015; Evans et al. 2018; Zdraljevic et al. 2019; Bernstein et al. 2019; Evans et al. 2020) have already been successfully used to screen toxicant responses and identify genetic factors that contribute to inter-individual differences in susceptibility.

C. elegans is a powerful whole-animal model for studying toxicant responses that has helped reveal the molecular mechanisms of toxicity for many compounds (Martinez-Finley and Aschner 2011; Hartman et al. 2021). Several features make *C. elegans* a good fit for identifying genes that cause differences in toxicant susceptibility with potential relevance to human health. First, conservation of genes and biological pathways between *C. elegans* and humans is high (Kaletta and Hengartner 2006), and toxicant responses in *C. elegans* are often predictive of responses in mammals (Boyd et al. 2016; Hunt 2017) and in standard ecotoxicological test species used in hazard assessment (Crombie et al. 2026). Second, *C. elegans* is easily reared in the laboratory, has a short lifecycle (Corsi et al. 2015), and several high-throughput phenotyping platforms have been developed that measure a range of toxicity endpoints, including fecundity (Andersen et al. 2015), development (Andersen et al. 2015; Widmayer et al. 2022), and behavior (Boyd et al. 2007; Barlow et al. 2022). Third, the *Caenorhabditis* Natural Diversity Resource (CaeNDR) provides a public repository of genetically diverse strains, along with whole-genome sequences and genomic tools to help dissect traits, including traits relevant to toxicology (Crombie et al. 2024). Fourth, genetically diverse *C. elegans* strains exhibit significant differences in their responses to toxicants and a large proportion of that variation is attributable to genetic differences (Vertino et al. 2011; Andersen et al. 2015; Evans et al. 2018; Bernstein et al. 2019; Zdraljevic et al. 2019; Widmayer et al. 2022; Leuthner et al. 2024), enabling statistically powerful GWAS (Widmayer et al. 2022) to identify multiple genomic regions associated with natural differences in toxicant response (Vertino et al. 2011; Andersen et al. 2015; Evans et al. 2018; Bernstein et al. 2019; Zdraljevic et al. 2019; Evans et al. 2020).

A clear example of the translational potential of *C. elegans* research comes from a recent GWAS that identified natural variation in *dbt-1*, a gene involved in branched-chain amino acid metabolism, as a determinant of arsenic susceptibility (Zdraljevic et al. 2019). Subsequent experiments in human embryonic kidney cells (HEK293T) showed that natural variation in the human ortholog of *dbt-1* similarly mediates arsenic-induced changes in fatty acid metabolism, revealing a novel and conserved mechanism of toxicity that could contribute to population-level differences in human arsenic susceptibility (Zdraljevic et al. 2019). Here, motivated by the translational potential of *C. elegans*, we sought to uncover candidate susceptibility genes for 23 environmental toxicants with substantial human health implications. The 23 diverse compounds represent five use groups (metals, herbicides, fungicides, insecticides, and flame retardants) and were selected using criteria outlined in the Toxic Substances Control Act, as amended in 2016 by the Frank R. Lautenberg Chemical Safety for the 21st Century Act, which prioritizes compounds with significant human exposure potential, environmental persistence, and bioaccumulation tendencies, among others (US Congress 2016; McPartland et al. 2022). Additionally, we prioritized toxicants for which susceptibility is known to be genetically determined in *C. elegans*, based on previous dose-response experiments (Widmayer et al. 2022). To identify candidate susceptibility genes for these 23 environmental toxicants, we performed a GWAS using a cohort of 195

wild strains. Differences in toxicant susceptibilities among the strains were quantified using previously described high-throughput techniques (Widmayer et al. 2022; Shaver and Andersen 2025). In total, we identified 40 genomic regions that correlate variation in thousands of genes with differences in toxicant susceptibilities. Guided by heuristics informed by two decades of quantitative trait research in *C. elegans*, we identified and prioritized 22 actionable genomic regions containing 94 candidate genes that can be experimentally validated as susceptibility genes using the organism's robust genetic toolkit (Andersen and Rockman 2022). Future studies that link these genes to toxicant susceptibility could reveal conserved susceptibility genes with translational relevance, ultimately enhancing chemical risk assessment for humans.

Materials and methods
C. elegans strains

The 195 strains for the mapping panel (Table S1) were sourced from CaeNDR and selected based on 3 criteria (Crombie et al. 2024). First, we chose 11 strains (PD1074, CB4856, CX11314, DL238, ECA36, ECA248, ECA396, JU775, MY16, RC301, and XZ1516) because they were included in one or both of two recent dose-response assays (Widmayer et al. 2022; Shaver et al. 2023). Importantly, these dose-response assays used the same phenotyping platform as this study, which allows for direct comparisons of experimental results. In CaeNDR, strains that share alleles at 99.997% of variant sites are grouped into genome-wide haplotypes called isotypes. Of the 11 strains referenced above, two (PD1074 and ECA248) are referred to by their isotype names (N2 and CB4855, respectively) in our analyses (Yoshimura et al. 2019; Ichikawa et al. 2025). All but three of the remaining 184 strains in the mapping panel were chosen based on the second criterion, assessments of detection power and false discovery rate (FDR), that were made using the NemaScan (9263c98) simulation profile, which is an open-source pipeline for GWAS mapping in *C. elegans* (Widmayer et al. 2022). In general, as the number of strains included in a mapping panel increases, the power of GWAS to detect simulated causal variants increases and the FDR decreases. Moreover, mapping panels with less population structure have substantially reduced FDR (Widmayer et al. 2022). For these reasons, we chose the largest mapping panel that we could phenotype at high replication (192 strains). To optimize the strain composition of the mapping panel, we generated 50 different hypothetical 192 strain mapping panels by randomly sampling 181 strains to pair with the 11 strains chosen above. We then assessed differences among the 50 mapping panels in detection power and FDR across a range of simulated causal variants. We simulated 30 traits per strain panel, each with narrow-sense heritabilities of 0.2, 0.5, or 0.8. For each trait, variation was attributed to five causal variants with minor allele frequencies (MAF) above 0.05. The effect size of each causal variant was randomly sampled from a gamma distribution. Ultimately, we chose the mapping panel with the best combination of high detection power and low FDR (Fig. S1). Finally, we included 3 additional strains (AB1, MY1, and PB306) to increase overlap with the *Caenorhabditis elegans* Multiparental Experimental Evolution (CeMEE) panel to better enable future comparisons of GWAS results across strain resources (Noble et al. 2017). All nematode strains were maintained at 20°C on 6 cm plates with modified nematode growth medium (NGMA), containing 1% agar and 0.7% agarose to prevent burrowing (Andersen et al. 2014). The NGMA plates were seeded with the

Escherichia coli strain OP50 as a nematode food source. All strains were grown for three generations without starvation on NGMA plates before toxicant exposure to reduce the transgenerational effects of starvation.

Liquid culture bacterial food preparation

Three large batches of HB101 *E. coli* were prepared as a food source for liquid culture of nematodes during toxicant exposures. For each batch of food, a starter culture was seeded with a single bacterial colony and grown in a sterile culture tube with 5 ml of 1X Horvitz Super Broth (HSB) at 37°C with shaking at 180 rpm. After 18 h, the optical density of the seed culture was measured (OD_{600}) and used to inoculate 14 4 L culture flasks at an initial OD_{600} value of 0.001 in 1 L of 1X HSB. These cultures were then grown at 37°C with shaking at 180 rpm for 15 h. Afterwards, the culture flasks were moved to 4°C to arrest growth, and the bacterial cells were washed as previously described (Widmayer et al. 2022). Finally, the washed bacterial cells for all 14 culture flasks were resuspended in K medium (51 mM NaCl, 32 mM KCl, 3 mM $CaCl_2$, 3 mM $MgSO_4$, 1.25 µg/ml Cholesterol) (Boyd et al. 2009) and combined at a final OD_{600} value of 100 as a single batch, aliquoted into 15 ml conicals, and frozen at -80°C for later use. To avoid batch effects caused by subtle differences in bacterial growth dynamics, frozen aliquots from each of the 3 batches were thawed and mixed in equal proportions prior to all feedings, as done previously (Gouveia et al. 2021).

Toxicant stock preparation

We prepared stock solutions of all toxicants with water or dimethyl sulfoxide (DMSO), depending on the aqueous solubility of the toxicant. The exact sources, catalog numbers, stock concentrations, and preparation notes for each of the toxicants are provided (Table S2). Following preparation of the toxicant stock solutions, they were aliquoted to microcentrifuge tubes and stored at -20°C for use in the high-throughput toxicant response assay. The exposure concentration used for each toxicant in the GWAS was taken from the dose with the highest heritability estimate in a recent dose-response assay (Widmayer et al. 2022). We also chose to include a low and high dose for some toxicants in the GWAS (Table S2). A secondary dose was included in the GWAS only if the rank order of strain responses deviated between high and low exposure concentrations in the Widmayer et al. dose-response assay and narrow-sense heritability estimates were greater than 0.2 for both doses. The logic for including both doses is that distinct genetic mechanisms could underlie the differential strain responses at the two concentrations tested.

Toxicant use groups and mechanisms of action (MoA)

We created toxicant assessment groups based on previously published use categories and mechanisms of action (MoA) data (Kramer et al. 2024). First, we queried the ECOTOXicology Knowledgebase (Olker et al. 2022) with toxicant CAS numbers to retrieve DSSToX Substance Identifiers (DTXSID), which we used to extract the chemical use and MoA data (Kramer et al. 2024). For use-based classification, we assigned the 23 toxicants to five distinct groups: Flame retardants ($N = 1$), fungicides ($N = 4$), metals ($N = 8$), herbicides ($N = 3$), and insecticides ($N = 7$) (Table S2). For three toxicants (mancozeb, paraquat, and silver nitrate), use category data were not available, and use groups were manually assigned based on information from regulatory and manufacturer documentation. Here, MoAs are defined as the dominant

initiating biochemical interactions between a toxicant and cellular targets that give rise to downstream effects. We applied the specific categories from Kramer et al. (2024), supplemented by additional references as needed, to group toxicants by shared MoA (Bus et al. 1976; Hughes 2002; Holt and Bard 2005; Chinalia et al. 2007; Lim et al. 2009; Plum et al. 2010; Macomber and Hausinger 2011; Gaetke et al. 2014; Roede and Jones 2014; Yao et al. 2021; Kang et al. 2024; Qu and Zheng 2024; Tao et al. 2024; Generalova et al. 2025). This approach yielded six MoA groups: Acetylcholinesterase (AChE) inhibition ($N = 6$), thiol binding ($N = 7$), redox cycling ($N = 3$), oxidative phosphorylation (OXPHOS) inhibition ($N = 4$), multiple mechanisms ($N = 1$), and other ($N = 5$) (Table S2). Thiol binding toxicants were defined as compounds whose primary MoA involves high-affinity binding to protein sulfhydryl groups, leading to broad enzyme inhibition. Lead lacks a single dominant initiating interaction and causes toxicity through several well supported mechanisms, including calcium mimicry, thiol binding, and mitochondrial disruption, which warrants a "multiple mechanisms" classification (Generalova et al. 2025). Toxicants that do not share a single dominant MoA with other compounds in the study were classified as "other" (Table S2).

High-throughput toxicant response assay

We measured toxicant response and control phenotypes for 195 strains across 28 experimental conditions (2 control conditions and 26 toxicant conditions) at high replication using a previously described high-throughput, image-based phenotyping assay (Widmayer et al. 2022; Shaver et al. 2023; Shaver and Andersen 2025). To accommodate the large number of treatments in our design (195 strains × 28 conditions = 5,460 treatments), we measured toxicant responses over 10 sequential experimental blocks. Each block contained all 28 experimental conditions. The first nine blocks contained 20 unique strains each and the 10th block contained 11 unique strains. Four strains (CB4856, JU775, MY16, and N2) were included in all 10 blocks to help estimate block effects. For each experimental block, strains were passaged for three generations, then bleach-synchronized in triplicate to account for any variation in development that might be attributed to the effect of bleach (Porta-de-la-Riva et al. 2012). Following bleach synchronization, approximately 30 embryos were transferred into the wells of 96-well microplates in 50 μL of K medium (Boyd et al. 2012). Embryos were exposed to toxicants using four biological replicates and three technical replicates (bleach groups) for a total of 12 wells per strain in each toxicant condition and experimental block. Embryos were exposed to the two control conditions, DMSO and water, using eight biological replicates and three technical replicates for a total of 24 wells per strain in each control condition and experimental block. The positions of the replicate wells were randomized across the microplates to control for any well position effects. After the embryos were added, microplates were labeled and sealed with gas-permeable sealing film (Fisher Cat #14-222-043), placed in humidity chambers, and incubated overnight at 20°C with shaking at 170 rpm. The following morning, food was prepared for the developmentally arrested first stage larval animals (L1s) using frozen aliquots of HB101 *E. coli* (section *Toxicant stock preparation*). HB101 aliquots were thawed at room temperature, combined into a single vessel, diluted to OD$_{600}$ 30 with K medium, and treated with kanamycin (final concentration 50 μM) to inhibit further bacterial growth and prevent contamination. Experimental treatments were prepared by adding toxicants or vehicle controls to the food suspension. For each block, all experimental treatments were prepared sequentially in random order and used immediately after preparation. All toxicant conditions were prepared at 3X concentration by thawing a frozen aliquot of toxicant stock solution, diluting it to a working concentration using DMSO or water if necessary, then mixing the required volume of the toxicant solution with OD$_{600}$ 30 HB101 food suspension in a sterile vessel. Depending on the toxicant, DMSO or water was added to ensure the final diluent concentration was 1% of the total volume. The synchronized L1 nematodes were simultaneously fed and treated by adding 25 μL of the 3X concentrated treatment suspension to the 50 μL of K medium in the microplate wells using a 12-channel micropipette. Immediately after feeding, the microplates were sealed with a gas-permeable sealing film (Fisher Cat #14-222-043), returned to the humidity chambers, and incubated for 48 h at 20°C with shaking at 170 rpm. Afterwards, the microplates were removed from the incubator and all wells were treated with 40.6 mM sodium azide (325 μL of 50 mM sodium azide in 1X M9) to paralyze and straighten the animals. After 10 min in sodium azide, well images were acquired using a Molecular Devices ImageXpress Nano microscope (Molecular Devices, San Jose, CA) with a 2X objective. The images were then used to measure toxicant response phenotypes.

Image processing, data cleaning, and toxicant susceptibility calculations

To rapidly extract toxicant response phenotypes from our well images, we wrote a Nextflow (v20.01.0) analysis pipeline that runs parallel instances of CellProfiler (v4.2.0) on the Quest High-Performance Computing Cluster (Northwestern University) (Di Tommaso et al. 2017; Stirling et al. 2021). The cellprofiler-nf (v1.1.0) workflow can be found at https://github.com/AndersenLab/cellprofiler-nf/tree/v1.1.0. At the core of this pipeline is CellProfiler's Worm Toolbox, which contains modules that facilitate the extraction of morphological features of individual *C. elegans* animals from images (Wählby et al. 2012). In brief, our pipeline identifies regions of interest (ROIs) in an image by segmenting them from the background via intensity thresholding. CellProfiler then uses the UntangleWorms module to find "nematode objects" within the ROIs using four probabilistic nematode models that we trained on similar data (Wählby et al. 2012; Nyaanga et al. 2021). The morphological features of the segmented ROIs and nematode objects found within the ROIs are then extracted using downstream measurement modules. The final output of our pipeline includes (1) a single R data file with image metadata, assay metadata, nematode object morphology measurements, and the parent ROI measurements for every nematode object found in the image set, and (2) a directory of diagnostic images that show the outlines of all the ROIs and nematode objects found in each image overlaid on the raw image. We ran the cellprofiler-nf pipeline on our experimental images and then cleaned and summarized the data using the *easyXpress* R package (v1.0.0) (Nyaanga et al. 2021). The data processing steps are summarized in the paragraph below, and a more detailed description is included in the supplemental material (**Methods S1**).

To clean potentially spurious measures from the raw data, we removed small objects (length < 100 μm), objects near the well edge, and objects for which multiple nematodes were detected within an ROI. For conditions that contained few or no small nematodes, we removed putatively spurious small objects < 165 μm. We then excluded all remaining objects that were classified as "non-nematode" by a stochastic gradient boosted classifier that we trained to 89.6% accuracy with over 1,000 nematode objects from a broad range of experimental conditions using the *caret* R package (v6.0-92) (Kuhn 2008). Finally, within each well, we removed nematode objects with outlier lengths using Tukey's

fences (Tukey 1977). To summarize the cleaned data for each well, we calculated the total number of nematodes and the median animal length within each well. We then filtered the summarized well data by removing wells with fewer than five or more than 30 animal length measurements or wells with outlier median animal length values for any combination of strain and condition. Next, we normalized our data by subtracting the average median animal length in control conditions for each strain in each bleach from the median animal length in treatment wells for the same strain. This normalization allowed us to remove the effect of strain differences that we observed in control conditions, estimate strain-specific toxicant susceptibilities, and retain the effects of bleach in our data. Next, within each treatment condition, we estimated the effect size of each bleach using a linear model and removed bleaches with extreme effects. We then regressed out the remaining bleach effects by taking the residual values from a linear model of bleach effects that excluded the bleaches with extreme effects. We refer to these final, zero-centered residual values as "normalized length differences" and use them to analyze toxicant susceptibilities throughout the manuscript. Finally, we filtered all data for a strain in a particular treatment if fewer than three wells were retained after applying the filters above.

Heritability calculations

The total phenotypic variance (V_P) of a given toxicant response can be partitioned into genetic variance (V_G) and environmental variance (V_E) components ($V_P = V_G + V_E$). Broad-sense heritability (H^2) describes the proportion of phenotypic variation attributable to genetic variance. To estimate H^2 for each toxicant response, we fit a linear mixed-effects model to the phenotype data with strain coded as a random effect using the *lme4::lmer* function from the *lme4* (v1.1.27.1) package in R (Bates et al. 2015). We then extracted the effect of strain (V_G) and the residual variance (V_E) from the model and calculated H^2 with the equation $H^2 = V_G/(V_G + V_E)$. We estimated confidence intervals around the H^2 estimates using a parametric bootstrap approach implemented with the *lme4::bootMer* function from the *lme4* (v1.1.27.1) package in R. We also estimated narrow-sense heritability (h^2) or the proportion of phenotypic variation (V_P) attributable to just additive genetic variance (V_A), using a previously described method (Widmayer et al. 2022). Briefly, we made a genotype matrix for the GWAS strains using the hard-filtered variant call format (VCF) file from CaeNDR (Release 20220216) (Crombie et al. 2024). We then calculated the variance-covariance matrix (M_A) from the genotype matrix using the *sommer::A.mat* function from the *sommer* (v4.1.5) R package (Covarrubias-Pazaran 2016). Next, we estimated V_A using the linear mixed-effects model function *sommer::mmer* with strain as a random effect and M_A as the covariance matrix. Finally, we calculated h^2 and its standard error using the *sommer::vpredict* function.

Correlations between toxicant susceptibilities and the identification of extreme responders

To assess the consistency of strain susceptibilities to multiple toxicants, we conducted a pairwise correlation analysis. We used the *psych::corr.test* function from the *psych* (v2.4.12) package in R to calculate Spearman's rank correlation coefficients and applied a Bonferroni correction to adjust *P*-values. We visualized the correlation results and performed hierarchical clustering of the correlation matrix with the *pheatmap::pheatmap* function from the *pheatmap* (v1.0.12) package from R. We examined whether differences in susceptibility were more correlated when condition

pairs involved toxicants from the same group (use or MoA) by estimating the average correlation of within-group condition pairs and between-group condition pairs. To help contextualize comparisons across toxicant conditions, we quantified the relative toxicity of each condition as percent growth inhibition relative to controls. For each strain and condition, percent growth inhibition was calculated as $\%GI = 100 \times [1 - (Lexposed/Lcontrol)]$, where *Lexposed* and *Lcontrol* are the mean animal lengths under exposed and matched control conditions, respectively. For each toxicant condition, %GI values are summarized as the mean ± SD across all strains included in the GWAS (Table S2). To identify individuals with susceptibility that significantly deviated from the population mean, we applied a threshold of 2 standard deviations (SD). For each toxicant condition, we calculated the mean and SD of normalized length differences of all individuals. We then classified individuals with responses exceeding the mean normalized length difference by more than 2 SDs as minimally susceptible, and those individuals with responses below the mean by more than 2 SDs as highly susceptible.

Genome-wide association (GWAS) mappings

We applied the NemaScan (commit hash: B 58711369124885fb 90ce9c53b720313fa68f79b, container id: Andersenlab/nemascan : 20220407173056db3227) GWAS mapping pipeline (Widmayer et al. 2022) to identify susceptibility-associated genomic regions for all toxicant response traits. We conducted association mapping with biallelic SNVs from the *C. elegans* hard-filtered variant call format file (VCF) on CaeNDR (Release 20220216) (Crombie et al. 2024). The VCF was filtered to include SNVs with no missing genotypes and a minor allele frequency (MAF) of 5% in the mapping panel. To reduce redundancy and control for markers in linkage disequilibrium (LD), we further pruned SNVs using PLINK v1.9 (Purcell et al. 2007; Chang et al. 2015) with the *–indep-pairwise* 50 10 0.8 option. The remaining 14,852 SNVs served as markers in the association mapping. To test markers for association with individual differences in susceptibility, we employed 2 mapping algorithms from the Genome-wide Complex Trait Analysis (GCTA) software package (Yang et al. 2011): *–fastGWA-lmm-exact* (Inbred) and *–mlma-loco* (LOCO). Each algorithm used a sparse genetic relatedness matrix (GRM) to account for the relatedness among strains within a mixed-effects linear model (Yang et al. 2011). We constructed sparse matrices for the Inbred and LOCO (Leave-One-Chromosome-Out) mapping algorithms with *–make-grm-Inbred* (designed for inbred organisms) and the *–make-grm* method, respectively. The Inbred algorithm adjusts the genetic relatedness matrix to more accurately model inbred populations (Jiang et al. 2019), whereas the LOCO algorithm excludes variants on the chromosome containing the focal SNV from the relatedness matrix to prevent confounding by local linkage (Yang et al. 2014). To further control the potential increase in false discoveries caused by residual population structure, we performed eigendecomposition on the GRMs and included the first eigenvector as a covariate in the linear mixed model.

We performed eigendecomposition of the genotype matrix of marker SNVs to estimate the number of independent markers and used this value to define the eigen-based significance threshold. For each mapping approach, we defined susceptibility-associated regions by aggregating neighboring significant markers into a single region of interest. To account for extensive LD, each region was extended by an additional 50 markers. Finally, we merged regions associated with differences in susceptibility that were separated by fewer than 200 markers into a single region of interest. We identify each susceptibility-associated region by the

chromosome and position of the most significant SNV (*e.g.*, V : 1486141), referred to as the peak marker. We evaluated concordance between the GWAS methods (Inbred and LOCO) by comparing the susceptibility-associated regions that each algorithm detected. We detected a total of 79 regions: 40 with Inbred and 39 with LOCO. 42 susceptibility-associated regions (Inbred = 22, LOCO = 20) were detected exclusively by 1 method. The other regions were identified by both methods, meaning the associated genomic regions physically overlapped. Simulations of *C. elegans* GWAS show no significant difference in detection power or false discovery rates between the two methods (Widmayer et al. 2022). However, mappings performed with LOCO have higher genomic inflation, suggesting that the Inbred algorithm provides a better correction for population structure than LOCO (Widmayer et al. 2022). Therefore, we focused on the susceptibility-associated regions detected using the Inbred approach.

Estimating the effect sizes and the proportion of variation explained by susceptibility-associated regions

We estimated two parameters to characterize each susceptibility-associated region: The phenotypic effect size and the proportion of phenotypic variance explained. To estimate phenotypic effect size, we extracted the β coefficient from the linear mixed model used in the GWAS, which represents the change in normalized length differences between strains with differing alleles at the peak marker. To calculate the proportion of phenotypic variance explained by each region, we first fit a one-way ANOVA with normalized length difference as the response variable and allelic state at the peak marker for the region as the predictor. The proportion of phenotypic variance explained by each region was calculated as the ratio of the sum of squares for peak marker genotype (SS_{allele}) to the total sum of squares (SS_{total}) from the ANOVA model ($var.exp = SS_{allele}/SS_{total}$).

Identifying biological processes over-represented in susceptibility-associated regions

For each toxicant, we conducted a Gene Ontology (GO) term over-representation analysis on genes within each susceptibility-associated region (Boyle et al. 2004). First, we filtered the WormBase gene feature file (GFF) (PRJNA13758, WS283) (Sternberg et al. 2024) to include only genes entirely contained within each susceptibility-associated region (*i.e.*, genes where both the start and stop coordinates fell within interval boundaries). We then applied the *clusterProfiler:: EnrichGO* function from the *clusterProfiler* (v4.6.2) package in R (Wu et al. 2021) to test for over-representation of biological processes among genes contained within susceptibility-associated regions. To control for multiple hypothesis testing, we set a Bonferroni-adjusted *P*-value significance threshold of 0.05 and a *q*-value threshold of 0.05.

Identification of candidate genes from susceptibility-associated genomic regions

To identify the genes that are most likely to contribute to individual differences in susceptibility, we performed a fine-mapping analysis on each susceptibility-associated region identified by the GWAS. Fine mapping tests all biallelic SNVs within a region for association with susceptibility using the Inbred algorithm, rather than the limited set of marker SNVs used for GWAS. Candidate genes were identified in the fine-mapping data by focusing on genes containing SNVs that had *P*-values above a significance threshold (-$\log_{10}$(*P*-value) > 5), were not rare (> 0.05 MAF), were in moderate to strong LD with the peak GWAS marker

($r^2 > 0.75$), and were predicted to have high impact on gene function. We used the Variant Annotation tool from CaeNDR (Crombie et al. 2024) to classify the predicted consequences of each SNV on gene function as either high-impact (affects amino acids, start/stop codons, or splice sites) or as low-impact (all other variants). LD was measured between each SNV from the fine mapping and the peak marker from the GWAS using PLINK v1.9 (Purcell et al. 2007). To summarize the biological processes associated with the candidate genes identified through fine mapping, we assigned GO terms to each candidate gene with the *clusterProfile::groupGO* function (level = 5) from the *clusterProfiler* R package (v4.6.2) (Wu et al. 2021). We also performed a GO term over-representation analysis on the candidate gene set using the same method previously applied to the full gene sets from susceptibility-associated regions (section *Identifying biological processes over-represented in susceptibility-associated regions*).

Physical overlaps and LD between susceptibility-associated regions

We identified physical overlaps between susceptibility-associated regions for each pair of toxicant response traits. For each trait pair, we quantified the proportion of overlapping regions relative to the total number of regions identified for both traits using the formula: ($Regions_{overlapping}/(Regions_A + Regions_B)$). To examine whether any two overlapping regions were in LD, we calculated the pairwise correlation coefficient (r^2) between peak markers from each region using PLINK (v1.9) (Purcell et al. 2007).

Semantic similarity of genes associated with differences in susceptibility

For each toxicant condition pair, we measured the functional similarity of genes within susceptibility-associated regions with GO term semantic similarity analysis. We used the *GoSemSim:: mClusterSim* function from the *GoSemSim* (v2.24.0) package in R (Yu et al. 2010) to calculate the functional similarity of genes from the graph structure of the GO terms (Wang et al. 2007). We conducted this analysis with two gene sets: All genes within any susceptibility-associated regions for each toxicant condition, and with candidate genes identified within these regions. We restricted our analysis to gene features from the WormBase GFF (PRJNA13758, WS283) (Sternberg et al. 2024) contained entirely within all susceptibility-associated regions detected for each toxicant. Biological process GO terms were sourced from the org. Ce.eg.db database (v3.16.0) (Carlson 2019) after converting gene IDs from Ensembl to Entrez with the *clusterProfiler::bitr* function from the *clusterProfiler* R package (v4.6.2) (Wu et al. 2021). Semantic similarity analysis was performed with the *GoSemSim::mClusterSim* function using the best-match average (BMA) method, which specifies how to handle genes with multiple GO terms. To visualize results and perform hierarchical clustering of toxicant traits by gene content similarity, we used the *pheatmap::pheatmap* function from the *pheatmap* (v1.0.12) package in R.

Prioritization of susceptibility-associated regions for additional follow-up

We manually reviewed all susceptibility-associated regions and developed a prioritization scheme by considering the following criteria. First, we excluded regions where fewer than 20 strains carried the minor allele at the peak marker. This criterion ensures that a sufficiently large set of phenotypically and genetically distinct individuals were available to validate effects and narrow regions of interest using subsequent crosses (Andersen and Rockman 2022). Next, we implemented a prioritization

scheme to rank the regions that remained ($n = 22$) from most actionable (1) to least actionable (22) by considering the following characteristics. The first metric in our prioritization scheme was the significance of association. Susceptibility-associated regions with higher peak marker -log10(*P*-values) were prioritized above those regions with less significant signatures of association. The second metric in our prioritization scheme was the extent of LD within each susceptibility-associated region. Large genomic regions of interest, with many variants in high LD, are more challenging to narrow to single-gene resolution because of their physical size and the strong linkage between alleles (Andersen and Rockman 2022). Therefore, we prioritized smaller genomic regions where the signature of association was localized around the peak marker. We classified fine mapping plots of susceptibility-associated regions into one of three categories (Less than 250 kb, 250 to 500 kb, or Greater than 500 kb) by considering the physical distance of significant markers in high LD ($r^2 > 0.5$) with the peak marker and prioritized regions categorized as Less than 250 kb or 250 to 500 kb. The final criterion was the overlap of each susceptibility-associated region with regions of extreme genetic diversity or hyper-divergent regions (HDRs). HDRs are shared by subsets of strains and often differ in gene content relative to the reference genome (Thompson et al. 2015; Kim et al. 2019; Lee et al. 2021; Moya et al. 2025). Because the exact genomic content of HDRs is unknown, a high incidence of HDRs within a susceptibility-associated region can complicate candidate gene identification. We located HDRs in each strain using features of short-read sequencing data (Methods S2), calculated the proportion of strains with at least one HDR overlapping each susceptibility-associated region, and prioritized regions where fewer strains carried overlapping HDRs. Human orthologs for candidate genes were identified using data from ortholist2 (Kim et al. 2018).

Results

Toxicant susceptibilities differ widely across 195 *C. elegans* wild strains

We used a high-throughput phenotyping platform to quantify the differences in susceptibility among 195 wild *C. elegans* strains. Synchronized first-larval-stage animals were exposed to each toxicant for 48 h in 96-well plates (section *High-throughput toxicant response assay*, Table S2). In control conditions, animals increase in length continuously as they develop (Knight et al. 2002; Nyaanga et al. 2022). However, exposure to toxicants reduces growth, and the magnitude of inhibition varies among strains. Growth inhibition was quantified for each strain as the average difference in mean body length between toxicant and control wells, thereby normalizing for inherent growth differences among strains. We then used zero-centered normalized length differences, which are residuals from a regression correcting for bleach effects (section *Image processing, data cleaning, and toxicant susceptibility calculations*), to compare susceptibility across strains for a given toxicant (Table S3). Strains with negative normalized length differences exhibited greater growth inhibition (higher susceptibility), whereas strains with positive values were less affected by the toxicant.

We found large differences in susceptibility among strains to particular toxicants (Fig. S2, Table S4). For example, normalized length differences ranged from -198 μm to 162 μm in mercury, reflecting large differences in the growth inhibition experienced by the most susceptible strain (ECA396) and the least susceptible strain (JU1934) (Fig. S2). In total, 108 strains displayed extreme susceptibilities relative to the rest of the population in at least

1 toxicant condition. High susceptibility (normalized length differences greater than two standard deviations below the mean) to a toxicant condition was more prevalent than minimal susceptibility (normalized length differences greater than two standard deviations above the mean) (Fig. S3, Table S4). The extent of differences in susceptibility among strains varied across toxicant conditions. The standard deviation (SD) of normalized length differences, which represents how much the average strain differed in susceptibility from the mean, ranged from ± 18 μm for silver 7.8 μM, the least variable condition, to ± 70 μm for mercury, the most variable condition (Fig. S2, Table S4). Notably, the variability in normalized length differences was generally similar across toxicant use groups (Table S5). Overall, the variability in toxicant susceptibilities suggests that genetic differences among the strains contribute to these responses.

Genetic differences among wild strains influence toxicant susceptibilities

To evaluate how genetic differences influence toxicant susceptibilities, we estimated broad-sense heritability (H^2) and narrow-sense heritability (h^2) for each toxicant condition (Fig. 1). Broad-sense heritability (H^2) reflects the proportion of variation in susceptibility explained by genetic differences among strains, including both individual variants with additive effects and non-additive genetic interactions between variants (such as epistatic and dominance effects). On average, these genetic factors collectively explained more than half the variance in susceptibility among strains (mean toxicant condition $H^2 = 0.53 \pm 0.16$ SD; Fig. 1, Table S6). Narrow-sense heritability (h^2), which captures only the proportion of variance in susceptibility attributable to additive genetic effects alone, was expectedly lower for all toxicant conditions (mean $h^2 = 0.21 \pm 0.13$ SD; Fig. 1, Table S6). Importantly, the h^2 estimates are representative of what can be detected using a GWAS, which assumes all variants contribute to differences in susceptibility additively and does not model non-additive interactions (Yang et al. 2011). Ultimately, the high heritability estimates described here (mean $h^2 > 0.2$) suggest that GWAS will have sufficient statistical power to detect genomic regions associated with differences in toxicant susceptibility among strains.

The large proportion of differences in susceptibility attributable to genetic factors likely reflects our selection strategy for toxicant conditions. We specifically chose toxicant concentrations where differences in susceptibility had the highest heritability across a small panel of eight genetically diverse strains (Widmayer et al. 2022). From this prior assay, where multiple concentrations were tested for each toxicant, we selected the most heritable concentration for each toxicant to maximize our ability to detect specific genetic variants using GWAS. We assumed that genetic variation observed in the small panel of genetically diverse strains would reflect the heritability of toxicant susceptibilities across a larger population. To evaluate this assumption, we compared the heritability estimates made here using 195 strains with those estimates derived previously using just eight strains. We found significant positive correlations between the previous heritability estimates and our current heritability estimates across all 26 toxicant conditions (Fig. S4). These correlations demonstrate that preliminary screens of toxicity across a small panel of diverse strains can provide insights into the heritability of differences in susceptibility across a larger population.
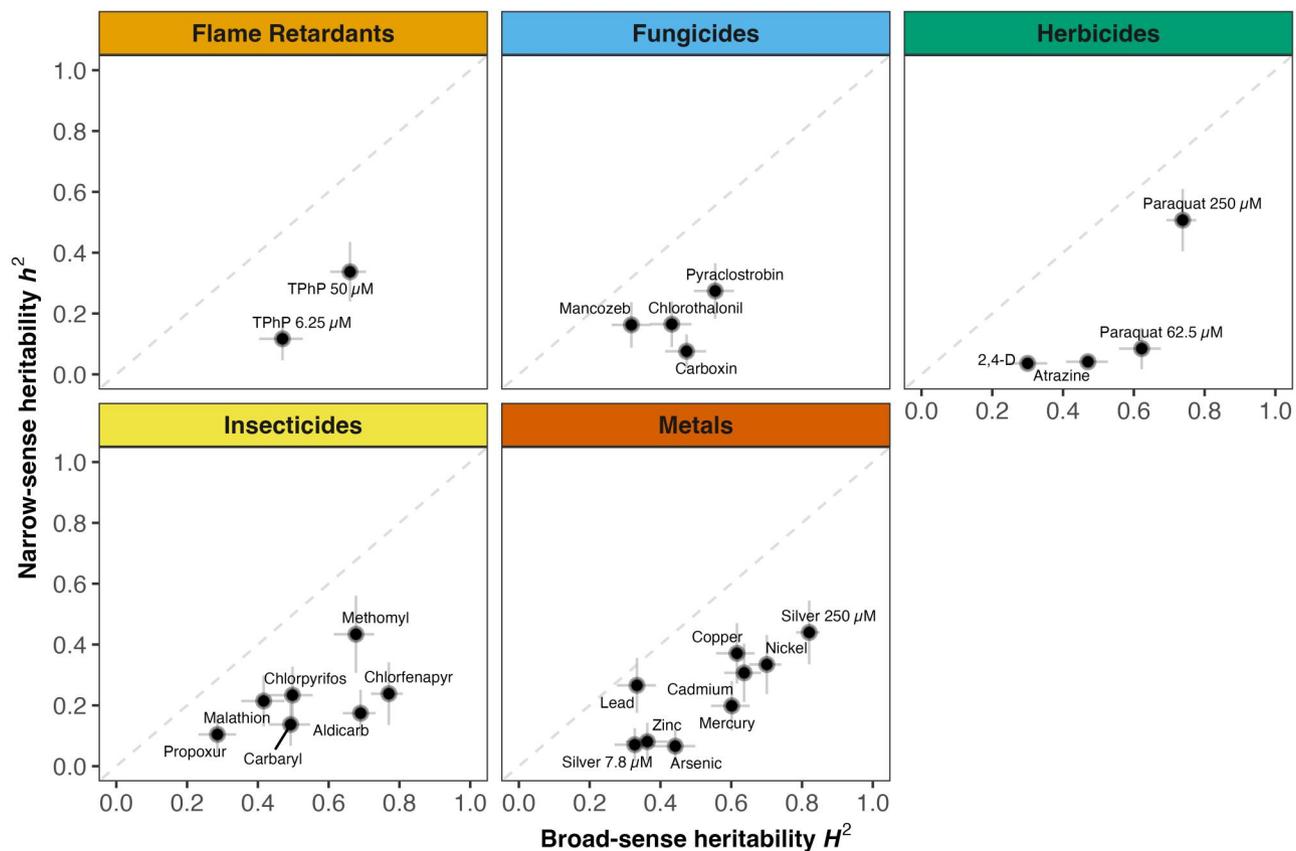
Fig. 1. Heritability of toxicant susceptibilities. The broad-sense (H^2) (x-axis) and narrow-sense heritability (h^2) (y-axis) of normalized length differences were calculated for each toxicant exposure condition. Within each use group, heritability estimates for a single toxicant exposure condition are denoted by a cross, where the horizontal line corresponds to the 95% confidence interval of the broad-sense heritability estimate obtained using the parametric bootstrapping approach, and the vertical line corresponds to the standard error of the narrow-sense heritability estimate. The three toxicants measured at two concentrations (TPhP, paraquat, and silver) are annotated with concentrations.

Strain response correlations point to mechanisms influencing susceptibility

Organisms rely on cellular stress response pathways to mitigate the harmful effects of toxicant exposures. In *C. elegans*, some of these pathways act generally across multiple toxicants (Shore and Ruvkun 2013; Blackwell et al. 2015; Labbadia and Morimoto 2015). By contrast, others are more specific. For example, the xenobiotic detoxification pathway contains proteins that target specific compounds, such as toxicants with similar chemical properties or mechanisms of action (MoA) (Hartman et al. 2021). We hypothesized that shared genetic variation in broadly acting stress response pathways could produce correlated strain susceptibility rankings across diverse toxicant conditions, although additional MoA-specific response pathways might yield stronger correlations among subsets of toxicants with similar MoAs. To test this hypothesis, we assessed how similarly strains responded to different toxicants by calculating pairwise Spearman's rank correlation coefficients of normalized length differences (section *Genome-wide association (GWAS) mappings*) (Spearman 1904). These coefficients (ρ) reflect the degree to which strain susceptibility rankings are consistent across toxicant pairs. Most condition pairs showed weak to moderate positive correlations (mean $\rho = 0.19 \pm 0.15$ SD), indicating that on average strains respond somewhat similarly across exposures (Fig. 2). Of the 325 possible toxicant condition pairs, 88 showed significant correlations, all of which were positive (Bonferroni-corrected *P*-value ≤ 0.05) (Fig. 2). These correlations were not

driven by a few extreme strains, because strains rarely displayed extreme responses across multiple toxicants (Fig. S3, Table S4). To visualize broader response patterns, we performed hierarchical clustering on the correlation matrix, which grouped toxicants by similarity in strain-level responses (section *Correlations between toxicant susceptibilities and the identification of extreme responders*). Overall, the correlations were modestly positive on average and toxicants were not cleanly grouped by shared MoA, consistent with the possibility that both general and toxicant-specific responses contribute to variation in susceptibility.

We further tested whether susceptibility correlations were stronger among toxicant conditions sharing use class, MoA, or similar overall toxicity (section *Toxicant use groups and mechanisms of action (MoA)* and *Correlations between toxicant susceptibilities and the identification of extreme responders*). Correlations among condition pairs from the same use group or MoA were not markedly stronger than correlations between different groups. For example, carbaryl (an insecticide) and carboxin (a fungicide) showed one of the highest correlations, despite differing in both use and MoA ($\rho = 0.69$, *P*-value < 0.0001; Fig. 2). The average correlation among within-use group pairs ($\rho = 0.24 \pm 0.14$ SD) was only slightly higher than between-use group pairs ($\rho = 0.18 \pm 0.15$ SD). Similarly, within- and between-MoA group pairs had comparable average correlations ($\rho = 0.24 \pm 0.14$ SD vs. $\rho = 0.18 \pm 0.15$ SD, respectively). Consistent with these findings, toxicants sharing use group or MoA were broadly distributed across the 2 major clusters (Fig. 2). However, the top-level split of the hierarchical clustering did separate AChE-inhibiting insecticides from redox-
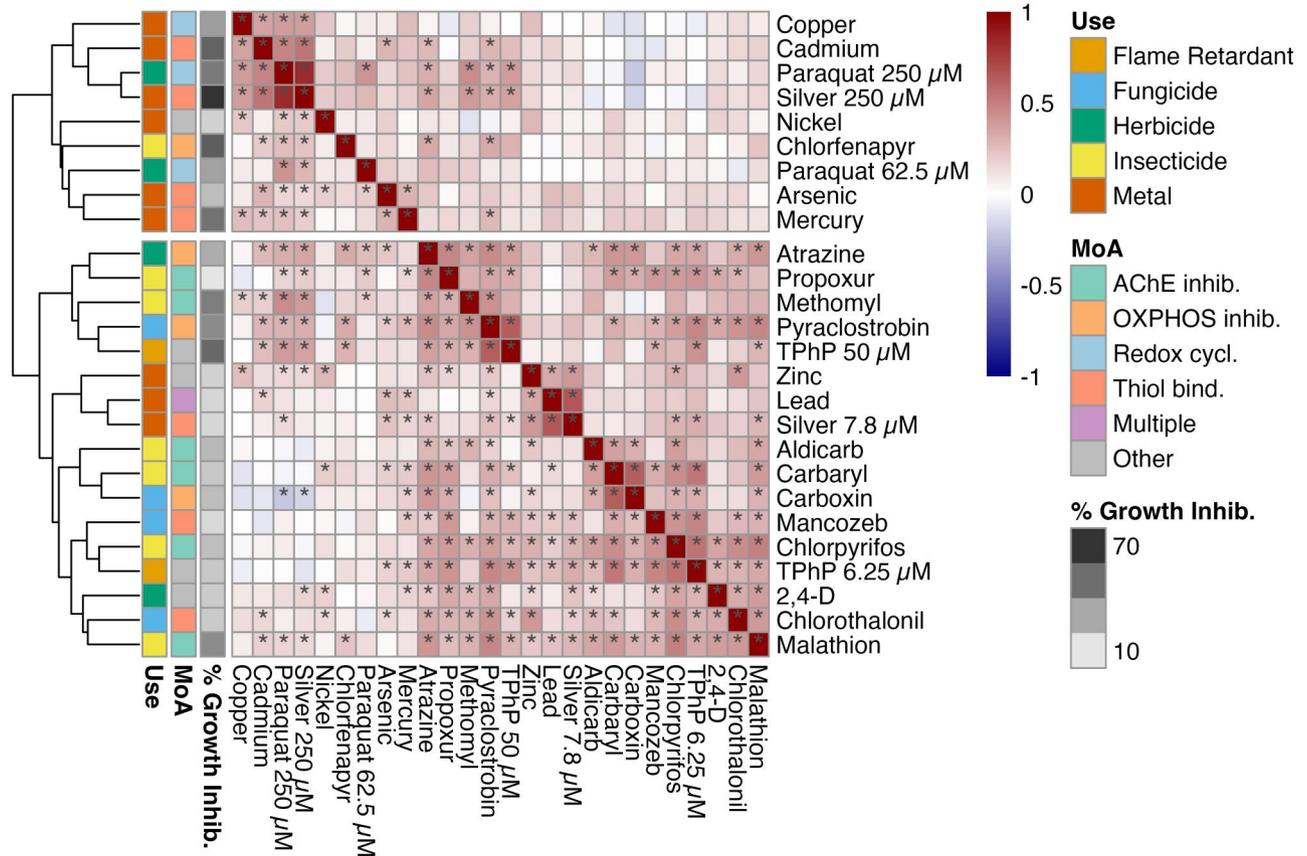
Fig. 2. Correlations between differences in susceptibility to toxicant conditions. The pairwise Spearman correlation coefficient (ρ) between all toxicant conditions is displayed as a correlation matrix and colored as a heatmap. Spearman's rank order correlation coefficients (colored cells), were calculated using the normalized length differences for all strains. Each cell represents the correlation between two toxicant conditions. The main diagonal shows self-correlations (ρ = 1) and divides the upper and lower triangles of the symmetrical correlation matrix. Significant correlations (P-value ≤ 0.05) are denoted with an asterisk (*). The upper right triangle shows significance symbols after Bonferroni multiple testing correction, and the lower left triangle shows uncorrected significance symbols. On the left, columns of colored tiles denote the use class, mechanism of action (MoA) and the mean percent growth inhibition (%GI) relative to controls for each toxicant condition (sections *Toxicant use groups and mechanisms of action (MoA)* and *Correlations between toxicant susceptibilities and the identification of extreme responders*). The toxicant conditions are ordered by hierarchical clustering based on Spearman correlation coefficients, such that conditions with more similar strain susceptibility rank orders are grouped together. The similarity between conditions is represented by the branch lengths in the dendrograms plotted to the left of the heatmap. The two major clusters resulting from the top-level split of the hierarchical clustering are emphasized by a horizontal division in the matrix.

cycling toxicants, which fell within the opposite major cluster (Fig. 2). To further contextualize cross-condition comparisons, we summarized each condition's effect magnitude as percent growth inhibition relative to controls (%GI) and evaluated its alignment with the hierarchical clustering (section *Correlations between toxicant susceptibilities and the identification of extreme responders*, Fig. 2, Tables S2). We did not observe clear clustering by %GI, as toxicant conditions spanning a wide range of inhibitory effects were distributed across both major clusters (Fig. 2). Moreover, conditions representing different concentrations of the same toxicant did not always cluster together (*e.g.*, 250 μM vs. 7.8 μM silver; Fig. 2), consistent with the possibility that more strongly inhibitory exposures might engage generalized responses alongside more MoA-specific responses, potentially affecting strain susceptibility rank orders.

GWAS detects genomic regions associated with differences in toxicant susceptibility

To more directly assess the genetic basis of susceptibility differences, we performed a GWAS of all toxicant conditions to pinpoint biological processes and candidate genes underlying strain-specific responses. Our GWAS approach used a representative

set of 14,852 marker SNVs distributed across the *C. elegans* genome to test for associations with susceptibility to each toxicant (section *Genome-wide association (GWAS) mappings*). This analysis identified 236 significant markers across 16 of the 26 toxicant conditions (Fig. S5). Because nearby markers often reflect the same signal of association, we grouped neighboring significant markers into 40 distinct genomic regions associated with susceptibility (Fig. 3, Table S7). For some analyses, we used the most significantly associated variant within each region as a representative marker, referred to as the "peak marker". Among the 16 toxicant conditions with significant associations, the number of detected regions ranged from 1 to 8, with a median of 1.5 (Table S7). The absolute effect sizes of the peak markers for each region ranged from 5 to 51 μm in normalized length difference, and the frequency of those variants in the GWAS population ranged from 5.1% to 47.9% (Fig. 4, Table S7, section *Estimating the effect sizes and the proportion of variation explained by susceptibility-associated regions*). Notably, peak markers with larger effects tended to occur at lower frequencies (Fig. 4), consistent with evolutionary expectations that alleles of large effect are maintained at low frequencies by selection (Orr 2005). For the 10 toxicant conditions without significant associations, susceptibility is likely
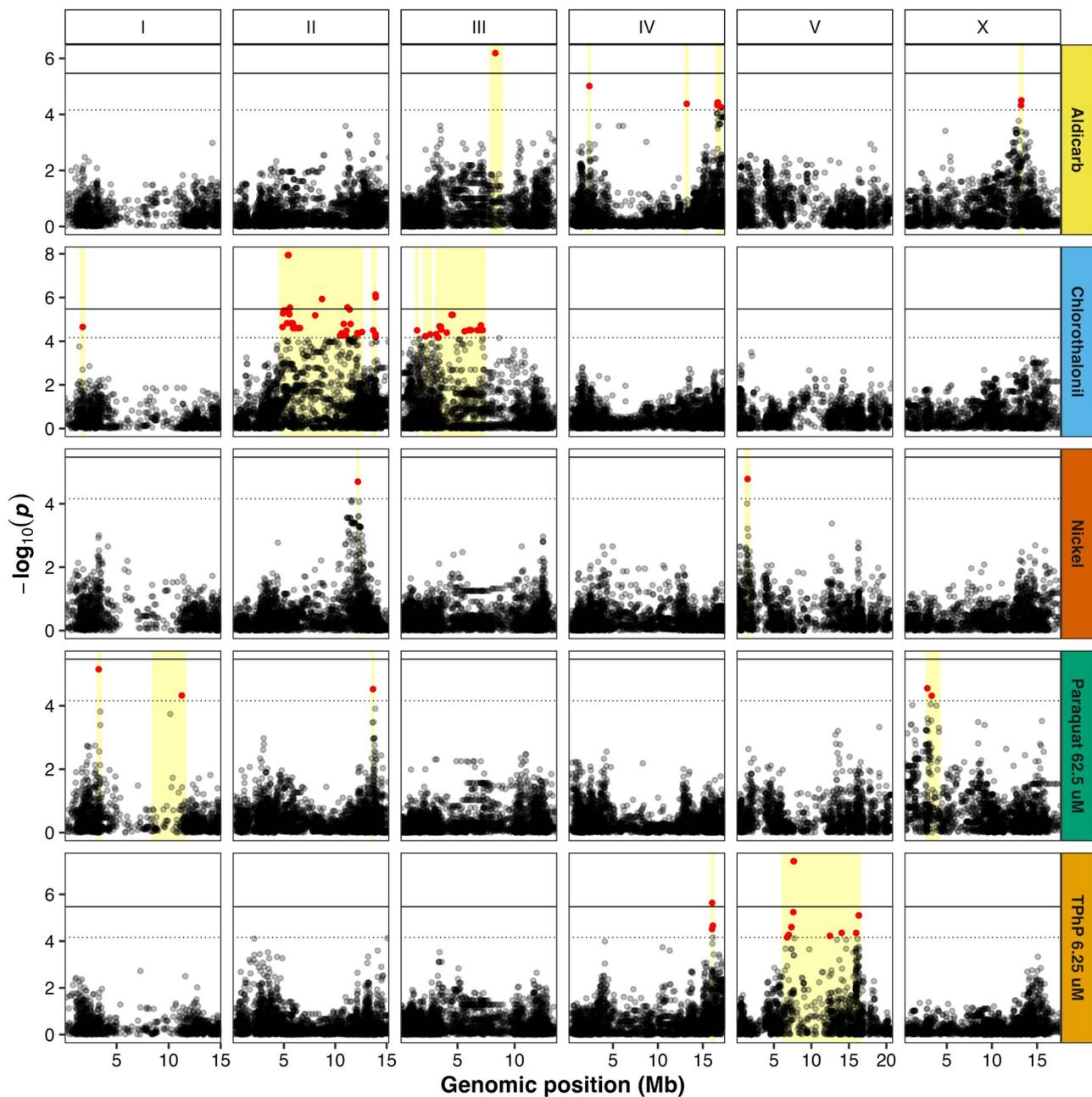
Fig. 3. Representative Manhattan plots showing 19 of 40 susceptibility-associated regions identified with GWAS. Representative genome-wide association mappings of normalized length differences for each toxicant use-group are shown. For each toxicant use-group, we selected a representative toxicant condition based on the heritability and the presence of actionable susceptibility-associated regions. Each point represents a single-nucleotide variant (SNV) that is present in at least 5% of the wild strains exposed to each toxicant condition. Genomic coordinates are plotted (x-axis) against the log-transformed P-value of the test of association for each SNV (y-axis). The solid black line is the Bonferroni-corrected significance threshold (BF) using all markers. The dashed horizontal gray line is the Eigen-corrected P-value threshold using independent markers corrected for LD (genome-wide eigendecomposition significance threshold). Red points represent SNVs above the EIGEN significance threshold, whereas black points represent SNVs below that threshold. Yellow boxes represent distinct susceptibility-associated regions.

influenced by variants that either cause small effects, are rare, or participate in epistatic interactions, which are more difficult to detect with GWAS (Manolio et al. 2009).

Functional enrichment and candidate susceptibility genes within GWAS regions

To explore the biological function of 40 susceptibility-associated genomic regions, we analyzed their gene content. Gene ontology (GO) analysis revealed significant enrichment of specific biological processes within 19 susceptibility-associated regions across 11 different toxicant conditions (section *Identifying biological*

processes over-represented in susceptibility-associated regions, Fig. S6). Some of these regions were enriched for genes involved in biological processes known to participate in toxicant responses. For example, three overlapping genomic regions associated with different toxicants (arsenic, II : 13692527; chlorothalonil, II : 13921653; and paraquat 62.5 μM, II : 13675568) were enriched for genes involved in glutathione and sulfur compound metabolism (GO : 0006749 and GO: 0006790, respectively) (Fig. S6). Accordingly, nine glutathione-s-transferase (GST) genes, which encode key phase II detoxification enzymes in *C. elegans* (Hartman et al. 2021), are in these regions, suggesting that natural variation in detoxification
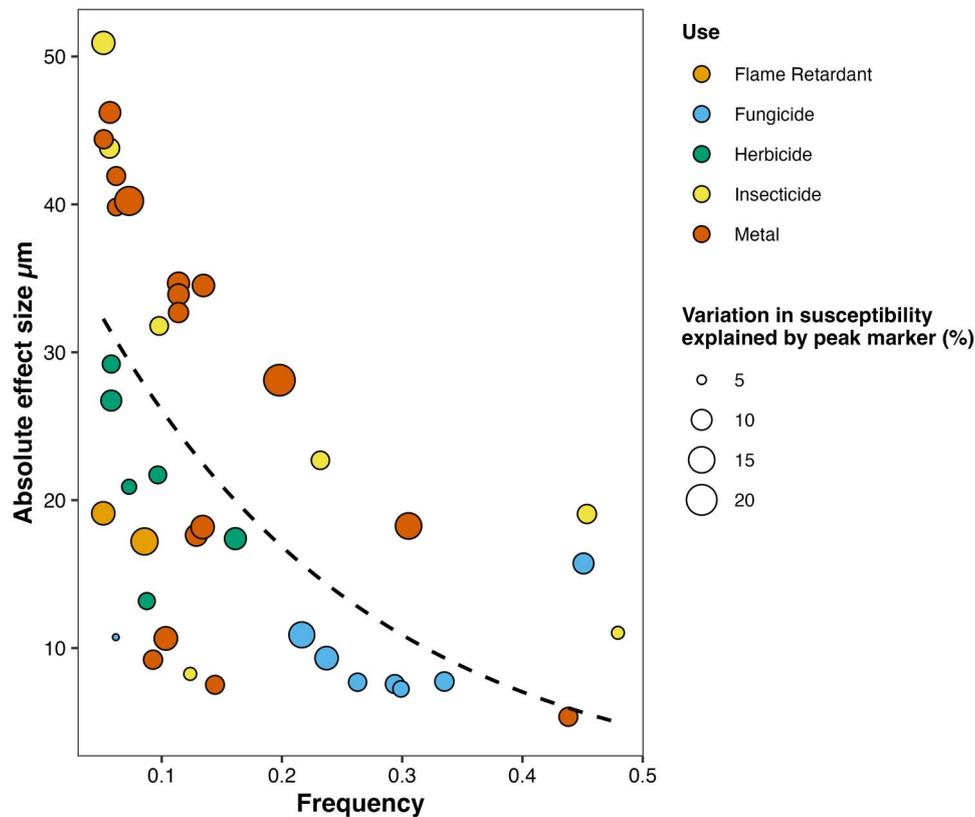
Fig. 4. Absolute effect size of susceptibility associated variants by frequency. Each point represents the most significant marker SNV (peak marker) from one of the 40 susceptibility-associated regions, plotted by its frequency in the 195 strains assayed (x-axis) and its absolute effect size (y-axis). The absolute effect size of each peak marker is calculated by taking the absolute value of the effect size estimated by the GWAS linear mixed model (β coefficient, section *Estimating the effect sizes and the proportion of variation explained by susceptibility-associated regions*). The effect size represents the additive effect of the SNV on the difference in normalized animal length between normalized length differences for strains with different alleles. The point size represents the proportion of variance in normalized animal length differences explained. The point colors indicate the toxicant use group. The dotted line represents the exponential decay fit of the relationship between frequency and absolute effect size for all peak markers.

pathways might contribute to differences in susceptibility to these toxicants. A different region associated with mercury (III : 3716201) was enriched for ubiquinone biosynthesis genes (GO : 0006743, GO : 0006744) (Fig. S6), consistent with reports that mercury disrupts mitochondrial electron transport in *C. elegans* (Ke et al. 2023). This region also contains *clk-1*, a conserved gene implicated in mitochondrial stress responses in both *C. elegans* and humans (Rodríguez-Aguilera et al. 2005; Monaghan et al. 2015). Yet another region (X: 2848181) associated with paraquat (62.5 μM) exposure was enriched for carbohydrate and hexose transport genes (GO : 0008643 and GO : 0008645, respectively), consistent with prior work that demonstrated glucose supplementation alleviates paraquat-induced developmental delays in *C. elegans* and mammalian cell lines (Wang et al. 2019) (Fig. S6). Importantly, other enriched biological processes revealed potential novel connections to toxicant responses.

Not all genes within associated regions are equally likely to influence susceptibility. Genes with variants predicted to impact protein function or transcription are more likely candidates to cause differences in susceptibility than those candidates without functional variation. We used statistical fine mapping combined with functional annotation of all variants within associated regions to prioritize candidate genes likely to contribute to susceptibility differences (section *Identification of candidate genes from susceptibility-associated genomic regions*). The complete fine-mapping and annotation results are provided in the Dryad archive (DOI:

https://doi.org/10.5061/dryad.cjsxksnmg, tables/full_fine_mapping. tsv). Using these criteria, we identified 136 candidate genes across 13 of the 16 toxicant conditions with at least one associated region (section *Identification of candidate genes from susceptibility-associated genomic regions*, Table S8). Several of these candidate genes have plausible connections to toxicant responses. For example, two nuclear hormone receptor (NHR) family members, *nhr-52* and *nhr-121*, were candidate genes for mercury (Table S8). NHRs are known regulators of xenobiotic transcriptional responses in *C. elegans* (Hartman et al. 2021), and elevated expression of *nhr-121* and *nhr-176* has been linked to anthelmintic drug exposure (Dube et al. 2023). Additionally, a candidate gene for zinc, *zig-7*, was previously linked to aldicarb resistance in *C. elegans*, which might suggest a potential role in the mediation of multiple toxicant responses (Sieburth et al. 2005) (Table S8). However, no gene, including *zig-7*, was a candidate for more than one toxicant. This observation contrasts with the modest correlations in susceptibility across toxicants and suggests that variants in distinct genes could underlie responses to different toxicant conditions. Overall, these candidate genes represent compelling targets for future experimental validation.

Differences in susceptibility are associated with distinct genes and biological processes

To further investigate whether the same genes might contribute to differences in susceptibility to multiple toxicants, we examined the

physical overlap between susceptibility-associated genomic regions. We found that 70% (28/40) of regions physically overlapped with regions from other toxicant conditions (Fig. 5, Fig. S7). However, these overlaps were limited in scope because most regions overlapped with only one other region (median overlap = 1), and only 16.7% (20/120) of all possible toxicant pairs shared any overlapping regions (Fig. 5, Table S9). Furthermore, we found that the most significant markers from any two overlapping regions showed minimal LD (mean $r^2 = 0.0098$, section *Physical overlaps and LD between susceptibility-associated regions*, Table S9), supporting the notion that distinct genetic variants within the overlapping regions were associated with differences in susceptibility to each toxicant. Together, these findings demonstrate that, despite some overlaps of susceptibility-associated regions, the same genes are unlikely to influence susceptibility to multiple toxicants.

Although distinct genes were associated with differences in toxicant susceptibility, variants affecting different genes could still contribute to susceptibility differences across multiple toxicants if those genes participate in the same biological pathways. To investigate, we quantified the functional similarity of genes associated with different toxicants by comparing their GO terms (section *Semantic similarity of genes associated with differences in susceptibility*, Fig. S8A) (Wang et al. 2007). For each toxicant condition pair, a semantic similarity estimate provides a quantitative measure (ranging from 0 to 1) of how functionally related their associated gene sets are. A high semantic similarity score (near 1) indicates that genes associated with both toxicants are involved in similar biological processes, suggesting the potential of shared mechanisms driving toxicant susceptibility. Conversely, a lower score (near 0) indicates functionally distinct gene sets. Across toxicant condition pairs, the average semantic similarity was 0.675 ± 0.142 (Fig. S87A), suggesting some functional overlap among gene sets located within susceptibility-associated regions for different toxicants. However, when we refined our analysis to include only candidate genes from those regions, the average functional similarity was much lower (0.245 ± 0.102 SD, Fig. S8B). Our results show that regions identified by GWAS often contain genes involved in functionally related biological processes, but the specific candidate genes within those regions point to distinct genetic drivers of susceptibility across toxicants.

Identifying the genes that directly influence toxicant susceptibility will require targeted follow-up experiments to validate the effects of each susceptibility-associated region and refine candidate gene lists (Andersen and Rockman 2022). Some genomic regions are more amenable to approaches used by *C. elegans* researchers for these purposes. Therefore, we prioritized regions that passed our criteria for additional follow-up experiments (section *Prioritization of susceptibility-associated regions for additional follow-up*) and identified 22 regions from 11 different toxicant exposure conditions that included at least one region from every use group, except flame retardants (Table S10). Several toxicant conditions had multiple actionable regions, such as chlorothalonil (6), mercury (4), arsenic (2), aldicarb (2), and silver nitrate (7.8 μM) (2) (Table S10). The broad representation of toxicants
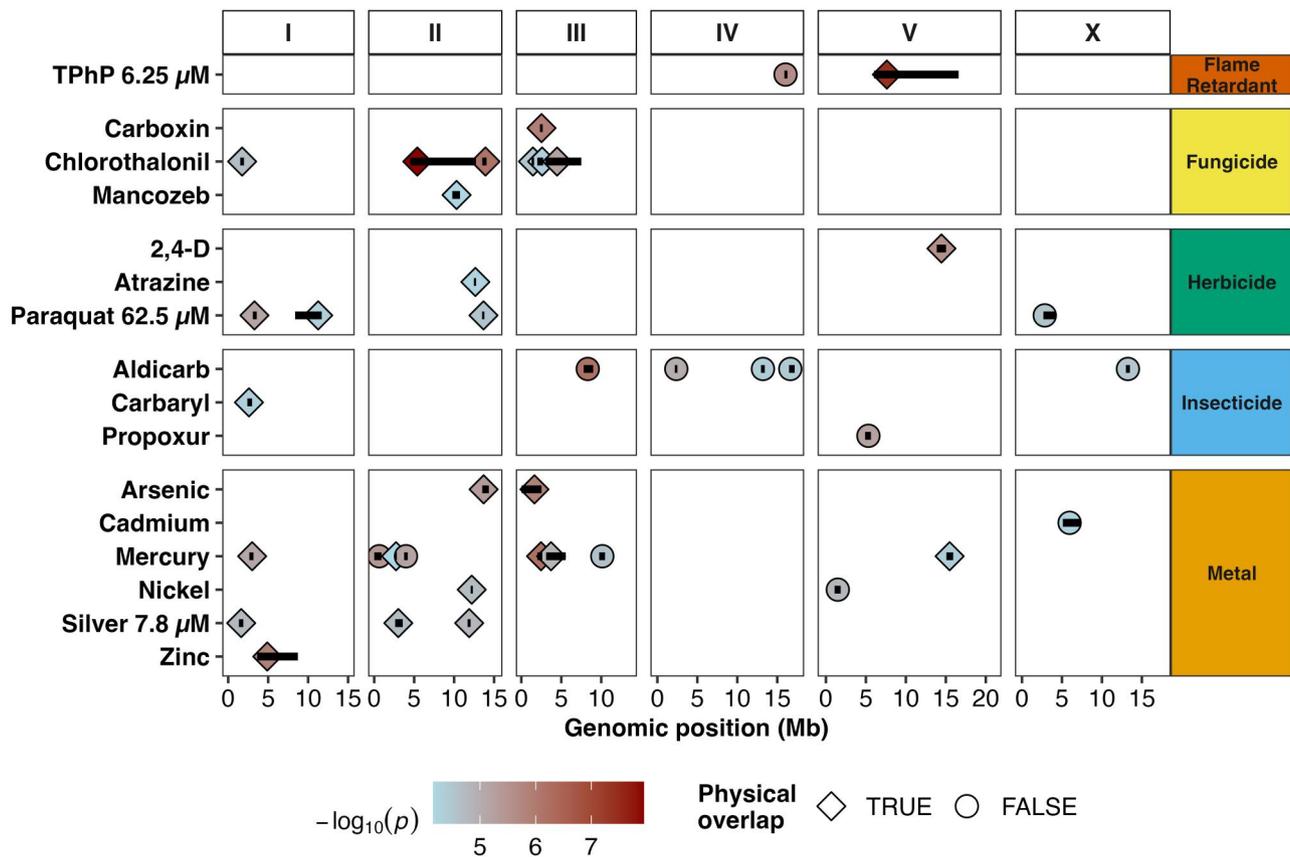

Fig. 5. Physical overlaps of genomic regions associated with susceptibility across toxicants. The susceptibility-associated regions for toxicant conditions with at least one marker above the eigen significance threshold are displayed by genomic position (Mb). Each region is represented by a horizontal black bar along its genomic span. The peak marker from each region is shown as a symbol colored according to its significance (-$\log_{10}$(P-value)). Diamond-shaped symbols indicate regions that physically overlap with at least one other genomic region associated with a different toxicant condition, whereas circles represent non-overlapping regions. Toxicant conditions are grouped on the y-axis by use classification (Flame Retardant, Fungicide, Herbicide, Insecticide, and Metal) and displayed across the six *C. elegans* chromosomes (I, II, III, IV, V, and X) on the x-axis.

with candidate genes underscores the power of *C. elegans* GWAS for identifying susceptibility-associated regions and candidate susceptibility genes that can be readily validated. Of the 136 candidate genes identified, 94 fell within actionable regions, including 44 with human orthologs (Table S11). Natural variation in these genes represents a high-priority target for future experimental validation (Table S8).

Discussion

Our investigation of toxicant responses across 195 genetically diverse *C. elegans* strains revealed substantial natural variation in susceptibility with genetic factors accounting for approximately half of the observed differences among strains (mean $H^2 = 0.53$). Using GWAS, we identified 40 genomic regions associated with differences in susceptibility, encompassing genes in both established toxicant-response pathways and novel biological processes previously unlinked to toxicant susceptibility. We applied prioritization criteria to highlight 22 high-priority genomic regions, which contain 94 candidate susceptibility genes recommended for experimental validation using proven strategies (Andersen and Rockman 2022). To the best of our knowledge, the majority of the candidate genes (80/94) have not yet been associated with toxicant responses. Moreover, almost half of these genes (44/94) have known human orthologs (Kim et al. 2018). These results reinforce the value of *C. elegans* as a robust whole-animal model for the discovery of candidate genes that contribute to differences in toxicant susceptibilities. Ultimately, validation of these candidate susceptibility genes will advance our understanding of the molecular mechanisms that drive toxicant responses with strong translational potential to improve human risk assessments.

Although GWAS is a powerful tool for identifying genetic variants associated with toxicant susceptibility, it cannot capture all the genetic factors influencing these traits. In our study, as in many others, a substantial portion of heritable variation remains unexplained, an observation often referred to as "missing heritability" (Maher 2008; Mayhew and Meyre 2017; Rockman 2012). This gap might come from the inherently low power of GWAS to detect rare variants, common variants with small effects, or non-additive interactions between variants that influence traits like toxicant susceptibility. For example, despite substantial narrow-sense heritability estimates for most toxicant susceptibilities in our study, we did not detect associated variants for 10 of the 26 toxicant conditions. Importantly, the detection of rare variants, common small effect variants, and non-additive interactions among variants is most straightforward in tractable model systems (Ehrenreich et al. 2012; Bloom et al. 2015), including *C. elegans* using established crossing and mapping schemes (Gaertner et al. 2012; Noble et al. 2017; Evans et al. 2018; Hahnel et al. 2018; Evans et al. 2021; Andersen and Rockman 2022; Zhang et al. 2022). Future investigations that employ these techniques might identify additional candidate susceptibility genes for the toxicants tested here and other high-priority environmental toxicants. Furthermore, as genomic resources continue to expand, including long-read assemblies that can accurately resolve variation in HDRs (Thomas et al. 2015; Lee et al. 2021; Stevens et al. 2022), future studies can build on this foundation to better characterize the genetic factors that influence toxicant susceptibility and extend these insights across species.

Our prioritization scheme for candidate susceptibility genes is constrained by the resolution of SNV mapping and the assumptions built into our selection criteria. Each region that we identified might harbor insertions, deletions, copy-number, or non-coding variants that influence gene function (Evans and Andersen 2020). These variants could also drive toxicant susceptibility traits but are undetectable by our current approach, which only considers SNVs and prioritizes SNVs that alter protein-coding sequences. Moreover, LD among nearby variants can obscure causal relationships, as correlated SNVs often share association signals and can mask the presence of multiple causal variants within a region (Cutter and Payseur 2013). Ultimately, integrating complementary data, including gene expression profiles and structural variant calls, together with mediation analyses (MacKinnon et al. 2007) that model causal relationships among genotype, gene expression, and phenotype (Evans and Andersen 2020; Zhang et al. 2022), will be critical for capturing the full spectrum of variants contributing to toxicant susceptibility.

Future work can translate *C. elegans* discoveries to human toxicology. First, the candidate susceptibility genes described here need to be functionally validated using experimental crosses and genetic tools such as CRISPR-Cas9 genome editing to confirm their role in toxicant response. Once validated, the human orthologs of these genes can be identified using established orthology databases (Kim et al. 2018; Emms and Kelly 2019). Population-scale human genomic datasets can then be used to characterize natural genetic variation in these orthologs across diverse human populations (Byrska-Bishop et al. 2022; Chen et al. 2024). Next, variants with predicted functional impacts can be introduced into CRISPR-edited human cell lines to evaluate their impacts on toxicant responses. Ultimately, the discovery of functionally important variants in human models can support the development of susceptibility biomarkers and improve chemical risk assessment by accounting for human genetic diversity.

Author contributions

Conceptualization: E.C.A. Data curation: R.M, T.A.C, N.D.M, A.O.S, J.B.C. Formal analysis: R.M, T.A.C. Funding acquisition: E.C.A. Investigation: R.M, T.A.C, S.J.W, J.W, J.B.C, R.E.T. Methodology: R.M, T.A.C, S.J.W, J.W, J.B.C. Project administration: E.C.A. Resources: E.C.A, R.E.T, C.B., L.S, L.V.S, M.V.R, M.G.S, M.-A.F. Software: T.A.C, S.J.W, R.M. Supervision: E.C.A. Validation: T.A.C, R.M. Visualization: T.A.C, S.J.W, R.M. Writing—original draft: T.A.C, R.M. Writing—reviewing & editing: T.A.C, R.M, S.J.W, E.C.A, A.O.S, J.W.

Supplementary material

Supplementary material is available at *Toxicological Sciences* online.

Conflicts of interest

None decalared.

Data availability

An archived, unmodifiable version of the data and code used in this study is available in the Dryad Digital Repository (DOI: https://doi.org/10.5061/dryad.cjsxksnmg). The repository, implemented using Quarto, contains all data, code, and rendered outputs required to reproduce the analyses. (https://github.com/AndersenLab/ToxinGWAS_Manuscript/tree/master).

References

Abdo N, Wetmore BA, Chappell GA, Shea D, Wright FA, Rusyn I. 2015. In vitro screening for population variability in toxicity of pesticide-containing mixtures. Environ Int. 85:147–155. https://doi.org/10.1016/j.envint.2015.09.012

Abdo N, Xia M, Brown CC, Kosyk O, Huang R, Sakamuru S, Zhou Y-H, Jack JR, Gallins P, Xia K, et al. 2015. Population-based in vitro hazard and concentration-response assessment of chemicals: The 1000 genomes high-throughput screening study. Environ Health Perspect. 123:458–466. https://doi.org/10.1289/ehp.1408775

Akhtar A. 2015. The flaws and human harms of animal experimentation. Camb Q Healthc Ethics. 24:407–419. https://doi.org/10.1017/S0963180115000079

Alam G, Jones BC. 2014. Toxicogenetics: in search of host susceptibility to environmental toxicants. Front Genet. 5:327. https://doi.org/10.3389/fgene.2014.00327

Andersen EC, Rockman MV. Natural genetic variation as a tool for discovery in caenorhabditis nematodes. Genetics. 2022 Jan 4;220 (1):iyab156. https://doi.org/10.1093/genetics/iyab156

Andersen EC, Rockman MV. 2022. Natural genetic variation as a tool for discovery in caenorhabditis nematodes. Genetics. 220. https://doi.org/10.1093/genetics/iyab156

Andersen EC, Shimko TC, Crissman JR, Ghosh R, Bloom JS, Seidel HS, Gerke JP, Kruglyak L. 2015. A powerful new quantitative genetics platform, combining Caenorhabditis elegans high-throughput fitness assays with a large collection of recombinant strains. G3. 5:911–920. https://doi.org/10.1534/g3.115.017178

Balik-Meisner M, Truong L, Scholl EH, La Du JK, Tanguay RL, Reif DM. 2018. Elucidating gene-by-environment interactions associated with differential susceptibility to chemical exposure. Environ Health Perspect. 126:067010. https://doi.org/10.1289/EHP2662

Barlow IL, Feriani L, Minga E, McDermott-Rouse A, O'Brien TJ, Liu Z, Hofbauer M, Stowers JR, Andersen EC, Ding SS, et al. 2022. Megapixel camera arrays enable high-resolution animal tracking in multiwell plates. Commun Biol. 5:253. https://doi.org/10.1038/s42003-022-03206-1

Barton NH, Keightley PD. 2002. Understanding quantitative genetic variation. Nat Rev Genet. 3:11–21. https://doi.org/10.1038/nrg700

Bates D, Mächler M, Bolker B, Walker S. 2015. Fitting linear mixed-effects models using lme4. J Stat Softw. 67:48. https://doi.org/10.18637/jss.v067.i01

Bernstein MR, Zdraljevic S, Andersen EC, Rockman MV. 2019. Tightly linked antagonistic-effect loci underlie polygenic phenotypic variation in C. elegans. Evol Lett. 3:462–473. https://doi.org/10.1002/evl3.139

Blackwell TK, Steinbaugh MJ, Hourihan JM, Ewald CY, Isik M. 2015. SKN-1/nrf, stress responses, and aging in Caenorhabditis elegans. Free Radic Biol Med. 88:290–301. https://doi.org/10.1016/j.freeradbiomed.2015.06.008

Bloom JS, Kotenko I, Sadhu MJ, Treusch S, Albert FW, Kruglyak L. 2015. Genetic interactions contribute less than additive effects to quantitative trait variation in yeast. Nat Commun. 6:8712. https://doi.org/10.1038/ncomms9712

Boyd WA, McBride SJ, Freedman JH. 2007. Effects of genetic mutations and chemical exposures on Caenorhabditis elegans feeding: evaluation of a novel, high-throughput screening assay. PLoS One. 2: E 1259. https://doi.org/10.1371/journal.pone.0001259

Boyd WA, Smith MV, Co CA, Pirone JR, Rice JR, Shockley KR, Freedman JH. 2016. Developmental effects of the ToxCast™ phase I and phase II chemicals in Caenorhabditis elegans and corresponding responses in zebrafish, rats, and rabbits. Environ Health Perspect. 124:586–593. https://doi.org/10.1289/ehp.1409645

Boyd WA, Smith MV, Freedman JH. 2012. Caenorhabditis elegans as a model in developmental toxicology. Methods Mol Biol. 889:15–24. https://doi.org/10.1007/978-1-61779-867-2_3

Boyd WA, Smith MV, Kissling GE, Rice JR, Snyder DW, Portier CJ, Freedman JH. 2009. Application of a mathematical model to describe the effects of chlorpyrifos on Caenorhabditis elegans development. PLoS One. 4: E 7024. https://doi.org/10.1371/journal.pone.0007024

Boyle EI, Weng S, Gollub J, Jin H, Botstein D, Cherry JM, Sherlock G. 2004. GO::TermFinder—open source software for accessing gene ontology information and finding significantly enriched gene ontology terms associated with a list of genes. Bioinformatics. 20:3710–3715. https://doi.org/10.1093/bioinformatics/bth456

Broekema RV, Bakker OB, Jonkers IH. 2020. A practical view of fine-mapping and gene prioritization in the post-genome-wide association era. Open Biol. 10:190221. https://doi.org/10.1098/rsob.190221

Bus JS, Cagen SZ, Olgaard M, Gibson JE. 1976. A mechanism of paraquat toxicity in mice and rats. Toxicol Appl Pharmacol. 35:501–513. https://doi.org/10.1016/0041-008x(76)90073-9

Byrska-Bishop M, Evani US, Zhao X, Basile AO, Abel HJ, Regier AA, Corvelo A, Clarke WE, Musunuri R, Nagulapalli K, et al. 2022. High-coverage whole-genome sequencing of the expanded 1000 genomes project cohort including 602 trios. Cell. 185:3426–3440. e19. https://doi.org/10.1016/j.cell.2022.08.004

Carlson M. org.Ce.eg.db. Bioconductor; 2019 [accessed 2024 Oct 24]. http://bioconductor.org/packages/org.Ce.eg.db/.

Chang CC, Chow CC, Tellier LC, Vattikuti S, Purcell SM, Lee JJ. 2015. Second-generation PLINK: rising to the challenge of larger and richer datasets. Gigascience. 4:7. https://doi.org/10.1186/s13742-015-0047-8

Chen S, Francioli LC, Goodrich JK, Collins RL, Kanai M, Wang Q, Alföldi J, Watts NA, Vittal C, Gauthier LD, et al. 2024. A genomic mutational constraint map using variation in 76,156 human genomes. Nature. 625:92–100. https://doi.org/10.1038/s41586-023-06045-0

Chinalia FA, Regali-Seleghin MH, Correa EM. 2007. 2, 4-D toxicity: cause, effect and control. Terrestr Aquat Environ Toxicol. 1:24–33.

Chiu WA, Rusyn I. 2018. Advancing chemical risk assessment decision-making with population variability data: challenges and opportunities. Mamm Genome. 29:182–189. https://doi.org/10.1007/s00335-017-9731-6

Church RJ, Wu H, Mosedale M, Sumner SJ, Pathmasiri W, Kurtz CL, Pletcher MT, Eaddy JS, Pandher K, Singer M, et al. 2014. A systems biology approach utilizing a mouse diversity panel identifies genetic differences influencing isoniazid-induced microvesicular steatosis. Toxicol Sci. 140:481–492. https://doi.org/10.1093/toxsci/kfu094

Co JY, Klein JA, Kang S, Homan KA. 2023. Toward inclusivity in preclinical drug development: a proposition to start with intestinal organoids. Adv Biol (Weinh). 7: E2200333. https://doi.org/10.1002/adbi.202200333

Corsi AK, Wightman B, Chalfie M. 2015. A transparent window into biology: A primer on caenorhabditis elegans. Genetics. 200 (2):387–407. https://doi.org/10.1534/genetics.115.176099

PMID:26088431. Erratum in: Genetics. 2015 Sep;201(1):339. https://doi.org/10.1534/genetics.115.180133

Covarrubias-Pazaran G. 2016. Genome-assisted prediction of quantitative traits using the R package sommer. PLoS One. 11: E0156744. https://doi.org/10.1371/journal.pone.0156744

Crombie TA, McKeown R, Moya ND, Evans KS, Widmayer SJ, LaGrassa V, Roman N, Tursunova O, Zhang G, Gibson SB, *et al.* 2024. CaeNDR, the caenorhabditis natural diversity resource. Nucleic Acids Res. 52:D850–D858. https://doi.org/10.1093/nar/gkad887

Crombie TA, Pamminger T, Andersen EC, Glaberman S. 2026. High-throughput toxicity screening with C. elegans: current platforms, key advantages, and future directions. Environ Sci Technol. 60:1560–1576. https://doi.org/10.1021/acs.est.5c12562

Cutter AD, Payseur BA. 2013. Genomic signatures of selection at linked sites: unifying the disparity among species. Nat Rev Genet. 14:262–274. https://doi.org/10.1038/nrg3425

Di Tommaso P, Chatzou M, Floden EW, Barja PP, Palumbo E, Notredame C. 2017. Nextflow enables reproducible computational workflows. Nat Biotechnol. 35:316–319. https://doi.org/10.1038/nbt.3820

Dube F, Hinas A, Delhomme N, Åbrink M, Svärd S, Tydén E. 2023. Transcriptomics of ivermectin response in Caenorhabditis elegans: integrating abamectin quantitative trait loci and comparison to the ivermectin-exposed DA1316 strain. PLoS One. 18: E0285262. https://doi.org/10.1371/journal.pone.0285262

Ehrenreich IM, Bloom J, Torabi N, Wang X, Jia Y, Kruglyak L. 2012. Genetic architecture of highly complex chemical resistance traits across four yeast strains. PLoS Genet. 8: E1002570. https://doi.org/10.1371/journal.pgen.1002570

Emms DM, Kelly S. 2019. OrthoFinder: phylogenetic orthology inference for comparative genomics. Genome Biol. 20:238. https://doi.org/10.1186/s13059-019-1832-y

Evans DM, Zhu G, Dy V, Heath AC, Madden PAF, Kemp JP, McMahon G, St Pourcain B, Timpson NJ, Golding J, *et al.* 2013. Genome-wide association study identifies loci affecting blood copper, selenium and zinc. Hum Mol Genet. 22:3998–4006. https://doi.org/10.1093/hmg/ddt239

Evans KS, Andersen EC. 2020. The gene scb-1 underlies variation in Caenorhabditis elegans chemotherapeutic responses. G3 (Bethesda). 10:2353–2364. https://doi.org/10.1534/g3.120.401310

Evans KS, Brady SC, Bloom JS, Tanny RE, Cook DE, Giuliani SE, Hippleheuser SW, Zamanian M, Andersen EC. 2018. Shared genomic regions underlie natural variation in diverse toxin responses. Genetics. 210:1509–1525. https://doi.org/10.1534/genetics.118.301311

Evans KS, Wit J, Stevens L, Hahnel SR, Rodriguez B, Park G, Zamanian M, Brady SC, Chao E, Introcaso K, *et al.* 2021. Two novel loci underlie natural differences in Caenorhabditis elegans abamectin responses. PLoS Pathog. 17: E 1009297. https://doi.org/10.1371/journal.ppat.1009297

Evans KS, Zdraljevic S, Stevens L, Collins K, Tanny RE, Andersen EC. 2020. Natural variation in the sequestosome-related gene, sqst-5, underlies zinc homeostasis in Caenorhabditis elegans. PLoS Genet. 16: E1008986. https://doi.org/10.1371/journal.pgen.1008986

Everman ER, Macdonald SJ. 2024. Gene expression variation underlying tissue-specific responses to copper stress in Drosophila melanogaster. G3 (Bethesda). 14: Jkae015. https://doi.org/10.1093/g3journal/jkae015

Ford LC, Jang S, Chen Z, Zhou Y-H, Gallins PJ, Wright FA, Chiu WA, Rusyn I. 2022. A population-based human in vitro approach to quantify inter-individual variability in responses to chemical mixtures. Toxics. 10:441. https://doi.org/10.3390/toxics10080441

Gaertner BE, Parmenter MD, Rockman MV, Kruglyak L, Phillips PC. 2012. More than the sum of its parts: a complex epistatic network underlies natural variation in thermal preference behavior in Caenorhabditis elegans. Genetics. 192:1533–1542. https://doi.org/10.1534/genetics.112.142877

Gaetke LM, Chow-Johnson HS, Chow CK. 2014. Copper: toxicological relevance and mechanisms. Arch Toxicol. 88:1929–1938. https://doi.org/10.1007/s00204-014-1355-y

Generalova A, Davidova S, Satchanska G. 2025. The mechanisms of lead toxicity in living organisms. J Xenobiot. 15:146. https://doi.org/10.3390/jox15050146

Gouveia GJ, Shaver AO, Garcia BM, Morse AM, Andersen EC, Edison AS, McIntyre LM. 2021. Long-term metabolomics reference material. Anal Chem. 93:9193–9199. https://doi.org/10.1021/acs.analchem.1c01294

Hahnel SR, Zdraljevic S, Rodriguez BC, Zhao Y, McGrath PT, Andersen EC. 2018. Extreme allelic heterogeneity at a Caenorhabditis elegans beta-tubulin locus explains natural resistance to benzimidazoles. PLoS Pathog. 14: E1007226. https://doi.org/10.1371/journal.ppat.1007226

Hanson KM, Long AD, Macdonald SJ. 2025. Extreme QTL mapping enables the identification of novel zinc toxicity response loci in Drosophila melanogaster. Genetics 231: iyaf173. https://doi.org/10.1093/genetics/iyaf173

Harrill AH, Desmet KD, Wolf KK, Bridges AS, Eaddy JS, Kurtz CL, Hall JE, Paine MF, Tidwell RR, Watkins PB. 2012. A mouse diversity panel approach reveals the potential for clinical kidney injury due to DB289 not predicted by classical rodent models. Toxicol Sci. 130:416–426. https://doi.org/10.1093/toxsci/kfs238

Harrill AH, Lin H, Tobacyk J, Seely JC. 2018. Mouse population-based evaluation of urinary protein and miRNA biomarker performance associated with cisplatin renal injury. Exp Biol Med (Maywood). 243:237–247. https://doi.org/10.1177/1535370217740854

Harrill AH, Watkins PB, Su S, Ross PK, Harbourt DE, Stylianou IM, Boorman GA, Russo MW, Sackler RS, Harris SC, *et al.* 2009. Mouse population-guided resequencing reveals that variants in CD44 contribute to acetaminophen-induced liver injury in humans. Genome Res. 19:1507–1515. https://doi.org/10.1101/gr.090241.108

Hartman JH, Widmayer SJ, Bergemann CM, King DE, Morton KS, Romersi RF, Jameson LE, Leung MCK, Andersen EC, Taubert S, *et al.* 2021. Xenobiotic metabolism and transport in Caenorhabditis elegans. J Toxicol Environ Health B Crit Rev. 24:51–94. https://doi.org/10.1080/10937404.2021.1884921

Holt KB, Bard AJ. 2005. Interaction of silver(I) ions with the respiratory chain of Escherichia coli: an electrochemical and scanning electrochemical microscopy study of the antimicrobial mechanism of micromolar Ag+. Biochemistry. 44:13214–13223. https://doi.org/10.1021/bi0508542

Hughes MF. 2002. Arsenic toxicity and potential mechanisms of action. Toxicol Lett. 133:1–16. https://doi.org/10.1016/s0378-4274(02)00084-x

Hunt PR. 2017. The *C. elegans* model in toxicity testing. J Appl Toxicol. 37:50–59. https://doi.org/10.1002/jat.3357

Ichikawa K, Shoura MJ, Artiles KL, Jeong D-E, Owa C, Kobayashi H, Suzuki Y, Kanamori M, Toyoshima Y, Iino Y, *et al.* 2025. CGC1, a new reference genome for Caenorhabditis elegans. Genome Res. 35:1902–1918. https://doi.org/10.1101/gr.280274.124

Jiang L, Zheng Z, Qi T, Kemper KE, Wray NR, Visscher PM, Yang J. 2019. A resource-efficient tool for mixed model association analysis of large-scale data. Nat Genet. 51:1749–1755. https://doi.org/10.1038/s41588-019-0530-8

Kaletta T, Hengartner MO. 2006. Finding function in novel targets: C. elegans as a model organism. Nat Rev Drug Discov. 5:387–398. https://doi.org/10.1038/nrd2031

Kang B, Wang J, Guo S, Yang L. 2024. Mercury-induced toxicity: mechanisms, molecular pathways, and gene regulation. Sci Total Environ. 943:173577. https://doi.org/10.1016/j.scitotenv.2024.173577

Ke T, Junior FB, Santamaria A, Bowman AB, Aschner M. 2023. Genetic factors in methylmercury-induced neurotoxicity: what have we learned from Caenorhabditis elegans models? Adv Neurotoxicol. 9:271–290. https://doi.org/10.1016/bs.ant.2023.01.006

Kim C, Kim J, Kim S, Cook DE, Evans KS, Andersen EC, Lee J. 2019. Long-read sequencing reveals intra-species tolerance of substantial structural variations and new subtelomere formation in C. elegans. Genome Res. 29:1023–1035. https://doi.org/10.1101/gr.246082.118

Kim W, Underwood RS, Greenwald I, Shaye DD. 2018. OrthoList 2: a new comparative genomic analysis of human and Caenorhabditis elegans genes. Genetics. 210:445–461. https://doi.org/10.1534/genetics.118.301307

Knight CG, Patel MN, Azevedo RBR, Leroi AM. 2002. A novel mode of ecdysozoan growth in caenorhabditis elegans. Evol Dev. 4:16–27. 10.1046/j.1525-142x.2002.01058.x

Koturbash I, Scherhag A, Sorrentino J, Sexton K, Bodnar W, Swenberg JA, Beland FA, Pardo-Manuel Devillena F, Rusyn I, Pogribny IP. 2011. Epigenetic mechanisms of mouse interstrain variability in genotoxicity of the environmental toxicant 1,3-butadiene. Toxicol Sci. 122:448–456. https://doi.org/10.1093/toxsci/kfr133

Kramer L, Schulze T, Klüver N, Altenburger R, Hackermüller J, Krauss M, Busch W. 2024. Curated mode-of-action data and effect concentrations for chemicals relevant for the aquatic environment. Sci Data. 11:60. https://doi.org/10.1038/s41597-023-02904-7

Kuhn M. 2008. Building predictive models in R using the caret package. J Stat Softw. 28:1–26. https://doi.org/10.18637/jss.v028.i05

Labbadia J, Morimoto RI. 2015. The biology of proteostasis in aging and disease. Annu Rev Biochem. 84:435–464. https://doi.org/10.1146/annurev-biochem-060614-033955

Lee D, Zdraljevic S, Stevens L, Wang Y, Tanny RE, Crombie TA, Cook DE, Webster AK, Chirakar R, Baugh LR, et al. 2021. Balancing selection maintains hyper-divergent haplotypes in Caenorhabditis elegans. Nat Ecol Evol. 5:794–807. https://doi.org/10.1038/s41559-021-01435-x

Leuthner TC, Zhang S, Kohrn BF, Stapleton HM, Baugh LR. 2024. Structure-specific variation in per- and polyfluoroalkyl substances toxicity among genetically diverse Caenorhabditis elegans strains. bioRxiv. https://doi.org/10.1101/2024.05.29.596269

Lim S, Ahn SY, Song IC, Chung MH, Jang HC, Park KS, Lee K-U, Pak YK, Lee HK. 2009. Chronic exposure to the herbicide, atrazine, causes mitochondrial dysfunction and insulin resistance. PLoS One. 4: E5186. https://doi.org/10.1371/journal.pone.0005186

MacKinnon DP, Fairchild AJ, Fritz MS. 2007. Mediation analysis. Annu Rev Psychol. 58:593–614. https://doi.org/10.1146/annurev.psych.58.110405.085542

Macomber L, Hausinger RP. 2011. Mechanisms of nickel toxicity in microorganisms. Metallomics. 3:1153–1162. https://doi.org/10.1039/c1mt00063b

Maher B. 2008. Personal genomes: the case of the missing heritability. Nature. 456:18–21. https://doi.org/10.1038/456018a

Manolio TA, Collins FS, Cox NJ, Goldstein DB, Hindorff LA, Hunter DJ, McCarthy MI, Ramos EM, Cardon LR, Chakravarti A, et al. 2009. Finding the missing heritability of complex diseases. Nature. 461:747–753. https://doi.org/10.1038/nature08494

Martinez-Finley EJ, Aschner M. 2011. Revelations from the nematode Caenorhabditis elegans on the complex interplay of metal toxicological mechanisms. J Toxicol. 2011:895236. https://doi.org/10.1155/2011/895236

Mayhew AJ, Meyre D. 2017. Assessing the heritability of complex traits in humans: methodological challenges and opportunities. Curr Genomics. 18:332–340. https://doi.org/10.2174/1389202918666170307161450

McPartland J, Shaffer RM, Fox MA, Nachman KE, Burke TA, Denison RA. 2022. Charting a path forward: assessing the science of chemical risk evaluations under the toxic substances control act in the context of recent national academies recommendations. Environ Health Perspect. 130:25003. https://doi.org/10.1289/EHP9649

Moksnes MR, Hansen AF, Wolford BN, Thomas LF, Rasheed H, Simić A, Bhatta L, Brantsæter AL, Surakka I, Zhou W, et al. 2024. A genome-wide association study provides insights into the genetic etiology of 57 essential and non-essential trace elements in humans. Commun Biol. 7:432. https://doi.org/10.1038/s42003-024-06101-z

Monaghan RM, Barnes RG, Fisher K, Andreou T, Rooney N, Poulin GB, Whitmarsh AJ. 2015. A nuclear role for the respiratory enzyme CLK-1 in regulating mitochondrial stress responses and longevity. Nat Cell Biol. 17:782–792. https://doi.org/10.1038/ncb3170

Moya ND, Yan SM, McCoy RC, Andersen EC. 2025. The long and short of hyperdivergent regions. Trends Genet. 41:303–314. https://doi.org/10.1016/j.tig.2024.11.005

Ng E, Lind PM, Lindgren C, Ingelsson E, Mahajan A, Morris A, Lind L. 2015. Genome-wide association study of toxic metals and trace elements reveals novel associations. Hum Mol Genet. 24:4739–4745. https://doi.org/10.1093/hmg/ddv190

Nguyen HT, Tsuchiya MCL, Yoo J, Iida M, Agusa T, Hirano M, Kim E-Y, Miyazaki T, Nose M, Iwata H. 2017. Strain differences in the proteome of dioxin-sensitive and dioxin-resistant mice treated with 2,3,7,8-tetrabromodibenzo-p-dioxin. Arch Toxicol. 91:1763–1782. https://doi.org/10.1007/s00204-016-1834-4

NIH to prioritize human-based research technologies. NIH Record. [accessed 2025 Oct 1]. https://nihrecord.nih.gov/2025/07/04/nih-prioritize-human-based-research-technologies.

Noble LM, Chelo I, Guzella T, Afonso B, Riccardi DD, Ammerman P, Dayarian A, Carvalho S, Crist A, Pino-Querido A, et al. 2017. Polygenicity and epistasis underlie fitness-proximal traits in the Caenorhabditis elegans multiparental experimental evolution (CeMEE) panel. Genetics. 207:1663–1685. https://doi.org/10.1534/genetics.117.300406

Nyaanga J, Crombie TA, Widmayer SJ, Andersen EC. 2021. easyXpress: an R package to analyze and visualize high-throughput C. elegans microscopy data generated using CellProfiler. PLoS One. 16: E0252000. https://doi.org/10.1371/journal.pone.0252000

Nyaanga J, Goss C, Zhang G, Ahmed HN, Andersen EJ, Miller IR, Rozenich JK, Swarthout IL, Vaughn JA, Mangan NM, et al. 2022. Changes in body shape implicate cuticle stretch in C. elegans growth control. Cells Dev. 170:203780. https://doi.org/10.1016/j.cdev.2022.203780

Olker JH, Elonen CM, Pilli A, Anderson A, Kinziger B, Erickson S, Skopinski M, Pomplun A, LaLone CA, Russom CL, et al. 2022. The ECOTOXicology knowledgebase: a curated database of ecologically relevant toxicity tests to support environmental research and risk assessment. Environ Toxicol Chem. 41:1520–1539. https://doi.org/10.1002/etc.5324

Orr HA. 2005. Theories of adaptation: what they do and don? t say. Genetica. 123:3–13. https://doi.org/10.1007/s10709-004-2702-3

Pierce BL, Kibriya MG, Tong L, Jasmine F, Argos M, Roy S, Paul-Brutus R, Rahaman R, Rakibuz-Zaman M, Parvez F, et al. 2012. Genome-

wide association study identifies chromosome 10q24.32 variants associated with arsenic metabolism and toxicity phenotypes in Bangladesh. PLoS Genet. 8: E1002522. https://doi.org/10.1371/journal.pgen.1002522

Plum LM, Rink L, Haase H. 2010. The essential toxin: impact of zinc on human health. Int J Environ Res Public Health. 7:1342–1365. https://doi.org/10.3390/ijerph7041342

Porta-de-la-Riva M, Fontrodona L, Villanueva A, Cerón J. 2012. Basic caenorhabditis elegans methods: synchronization and observation. J Vis Exp. 10:e4019. https://doi.org/10.3791/4019

Purcell S, Neale B, Todd-Brown K, Thomas L, Ferreira MAR, Bender D, Maller J, Sklar P, de Bakker PIW, Daly MJ, *et al.* 2007. PLINK: a tool set for whole-genome association and population-based linkage analyses. Am J Hum Genet. 81:559–575. https://doi.org/10.1086/519795

Qu F, Zheng W. 2024. Cadmium exposure: mechanisms and pathways of toxicity and implications for human health. Toxics. 12:388. https://doi.org/10.3390/toxics12060388

Rockman MV. 2012. The QTN program and the alleles that matter for evolution: all that's gold does not glitter. Evolution (N Y). 66:1–17. https://doi.org/10.1111/j.1558-5646.2011.01486.x

Rodríguez-Aguilera JC, Gavilán A, Asencio C, Navas P. 2005. The role of ubiquinone in Caenorhabditis elegans longevity. Ageing Res Rev. 4:41–53. https://doi.org/10.1016/j.arr.2004.09.001

Roede JR, Jones DP. 2014. Thiol-reactivity of the fungicide maneb. Redox Biol. 2:651–655. https://doi.org/10.1016/j.redox.2014.04.007

Rossi G, Manfrin A, Lutolf MP. 2018. Progress and potential in organoid research. Nat Rev Genet. 19:671–687. https://doi.org/10.1038/s41576-018-0051-9

Rusyn I, Chiu WA, Wright FA. 2022. Model systems and organisms for addressing inter- and intra-species variability in risk assessment. Regul Toxicol Pharmacol. 132:105197. https://doi.org/10.1016/j.yrtph.2022.105197

Rusyn I, Gatti DM, Wiltshire T, Kleeberger SR, Threadgill DW. 2010. Toxicogenetics: population-based testing of drug and chemical safety in mouse models. Pharmacogenomics. 11:1127–1136. https://doi.org/10.2217/pgs.10.100

Schmeisser S, Miccoli A, von Bergen M, Berggren E, Braeuning A, Busch W, Desaintes C, Gourmelon A, Grafström R, Harrill J, *et al.* 2023. New approach methodologies in human regulatory toxicology - not if, but how and when!. Environ Int. 178:108082. https://doi.org/10.1016/j.envint.2023.108082

Shaver AO, Andersen E. High-throughput larval development assay (HTLDA). protocols.io; 2025 Jul 16 [accessed 2025 Oct 20]. https://www.protocols.io/view/high-throughput-larval-development-assay-htlda-dxs77nhn.

Shaver AO, Wit J, Dilks CM, Crombie TA, Li H, Aroian RV, Andersen EC. 2023. Variation in anthelmintic responses are driven by genetic differences among diverse C. elegans wild strains. PLoS Pathog. 19: E1011285. https://doi.org/10.1371/journal.ppat.1011285

Shore DE, Ruvkun G. 2013. A cytoprotective perspective on longevity regulation. Trends Cell Biol. 23:409–420. https://doi.org/10.1016/j.tcb.2013.04.007

Sieburth D, Ch'ng Q, Dybbs M, Tavazoie M, Kennedy S, Wang D, Dupuy D, Rual J-F, Hill DE, Vidal M, *et al.* 2005. Systematic analysis of genes required for synapse structure and function. Nature. 436:510–517. https://doi.org/10.1038/nature03809

Spearman C. 1904. The proof and measurement of association between two things. Am J Psychol. 15:72. https://doi.org/10.2307/1412159

Sternberg PW *et al.* 2024. WormBase 2024: status and transitioning to alliance infrastructure. *Genetics*. 227:iyae050. https://doi.org/10.1093/genetics/iyae050

Stevens L, Moya ND, Tanny RE, Gibson SB, Tracey A, Na H, Chitrakar R, Dekker J, Walhout AJM, Baugh LR, *et al.* 2022. Chromosome-

level reference genomes for two strains of caenorhabditis briggsae: an improved platform for comparative genomics. Genome Biol Evol. 14:evac042. https://doi.org/10.1093/gbe/evac042

Stirling DR, Swain-Bowden MJ, Lucas AM, Carpenter AE, Cimini BA, Goodman A. 2021. CellProfiler 4: improvements in speed, utility and usability. BMC Bioinformatics. 22:433. https://doi.org/10.1186/s12859-021-04344-9

Tao H, Fang C, Xiao Y, Jin Y. 2024. The toxicity and health risk of chlorothalonil to non-target animals and humans: a systematic review. Chemosphere. 358:142241. https://doi.org/10.1016/j.chemosphere.2024.142241

Thomas CG, Wang W, Jovelin R, Ghosh R, Lomasko T, Trinh Q, Kruglyak L, Stein LD, Cutter AD. 2015. Full-genome evolutionary histories of selfing, splitting, and selection in caenorhabditis. Genome Res. 25:667–678. https://doi.org/10.1101/gr.187237.114

Thompson OA, Snoek LB, Nijveen H, Sterken MG, Volkers RJM, Brenchley R, Van't Hof A, Bevers RPJ, Cossins AR, Yanai I, *et al.* 2015. Remarkably divergent regions punctuate the genome assembly of the Caenorhabditis elegans Hawaiian strain CB4856. Genetics. 200:975–989. https://doi.org/10.1534/genetics.115.175950

Thunga P, Truong L, Rericha Y, Du JL, Morshead M, Tanguay RL, Reif DM. 2022. Utilizing a population-genetic framework to test for gene-environment interactions between zebrafish behavior and chemical exposure. Toxics. 10:769. https://doi.org/10.3390/toxics10120769

To KT, Kleinstreuer N, Vasiliou V, Hogberg HT. 2023. New approach methodologies to address population variability and susceptibility. Hum Genomics. 17:56. https://doi.org/10.1186/s40246-023-00502-7

Tsuchiya M, Ji C, Kosyk O, Shymonyak S, Melnyk S, Kono H, Tryndyak V, Muskhelishvili L, Pogribny IP, Kaplowitz N, *et al.* 2012. Interstrain differences in liver injury and one-carbon metabolism in alcohol-fed mice. Hepatology. 56:130–139. https://doi.org/10.1002/hep.25641

Tukey JW. 1977. Exploratory data analysis. Addison-Wesley Publishing Company. Reading, MA, USA.

US Congress. Frank R. lautenberg chemical safety for the 21st century act. Pub. L. No. 114-182, 130 Stat. 448 (114th Congress, 22 June 2016). 2016. https://www.congress.gov/114/plaws/publ182/PLAW-114publ182.pdf.

USEPA. Strategic plan to promote the development and implementation of alternative test methods within the TSCA program. June 22, 2018. Washington (DC): U.S. Environmental Protection Agency, Office of Chemical Safety and Pollution Prevention; 2018. https://www.epa.gov/sites/default/files/2018-06/documents/epa_alt_strat_plan_6-20-18_clean_final.pdf.

Vertino A, Ayyadevara S, Thaden JJ, Shmookler Reis RJ. 2011. A narrow quantitative trait locus in C. elegans coordinately affects longevity, thermotolerance, and resistance to paraquat. Front Genet. 2:63. https://doi.org/10.3389/fgene.2011.00063

Wahlberg KE, Guazzetti S, Pineda D, Larsson SC, Fedrighi C, Cagna G, Zoni S, Placidi D, Wright RO, Smith DR, *et al.* 2018. Polymorphisms in manganese transporters SLC30A10 and SLC39A8 are associated with children's neurodevelopment by influencing manganese homeostasis. Front Genet. 9:664. https://doi.org/10.3389/fgene.2018.00664

Wählby C, Kamentsky L, Liu ZH, Riklin-Raviv T, Conery AL, O'Rourke EJ, Sokolnicki KL, Visvikis O, Ljosa V, Irazoqui JE, *et al.* 2012. An image analysis toolbox for high-throughput C. elegans assays. Nat Methods. 9:714–716. https://doi.org/10.1038/nmeth.1984

Wang C, Zhang Y, Li F, Wei Y. 2019. Conserved roles of glucose in suppressing reactive oxygen species-induced cell death and animal survival. Aging (Albany NY). 11:5726–5743. https://doi.org/10.18632/aging.102155

Wang JZ, Du Z, Payattakool R, Yu PS, Chen C-F. 2007. A new method to measure the semantic similarity of GO terms. Bioinformatics. 23:1274–1281. https://doi.org/10.1093/bioinformatics/btm087

Wang Z, Walker GW, Muir DCG, Nagatani-Yoshida K. 2020. Toward a global understanding of chemical pollution: a first comprehensive analysis of national and regional chemical inventories. Environ Sci Technol. 54:2575–2584. https://doi.org/10.1021/acs.est.9b06379

Wheeler HE, Dolan ME. 2012. Lymphoblastoid cell lines in pharmacogenomic discovery and clinical translation. Pharmacogenomics. 13:55–70. https://doi.org/10.2217/pgs.11.121

Widmayer SJ, Crombie TA, Nyaanga JN, Evans KS, Andersen EC. 2022. C. elegans toxicant responses vary among genetically diverse individuals. Toxicology. 479:153292. https://doi.org/10.1016/j.tox.2022.153292

Widmayer SJ, Evans KS, Zdraljevic S, Andersen EC. 2022. Evaluating the power and limitations of genome-wide association studies in Caenorhabditis elegans. G3. 12. https://doi.org/10.1093/g3journal/jkac114

Wu T, Hu E, Xu S, Chen M, Guo P, Dai Z, Feng T, Zhou L, Tang W, Zhan L, et al. 2021. clusterProfiler 4.0: a universal enrichment tool for interpreting omics data. Innovation (Camb). 2:100141. https://doi.org/10.1016/j.xinn.2021.100141

Yang J, Lee SH, Goddard ME, Visscher PM. 2011. GCTA: a tool for genome-wide complex trait analysis. Am J Hum Genet. 88:76–82. https://doi.org/10.1016/j.ajhg.2010.11.011

Yang J, Zaitlen NA, Goddard ME, Visscher PM, Price AL. 2014. Advantages and pitfalls in the application of mixed-model association methods. Nat Genet. 46:100–106. https://doi.org/10.1038/ng.2876

Yao C, Yang H, Li Y. 2021. A review on organophosphate flame retardants in the environment: occurrence, accumulation, metabolism and toxicity. Sci Total Environ. 795:148837. https://doi.org/10.1016/j.scitotenv.2021.148837

Yoo HS, Bradford BU, Kosyk O, Shymonyak S, Uehara T, Collins LB, Bodnar WM, Ball LM, Gold A, Rusyn I. 2015. Comparative analysis of the relationship between trichloroethylene metabolism and tissue-specific toxicity among inbred mouse strains: liver effects. J Toxicol Environ Health Part A. 78:15–31. https://doi.org/10.1080/15287394.2015.958417

Yoshimura J, Ichikawa K, Shoura MJ, Artiles KL, Gabdank I, Wahba L, Smith CL, Edgley ML, Rougvie AE, Fire AZ, et al. 2019. Recompleting the Caenorhabditis elegans genome. Genome Res. 29:1009–1022. https://doi.org/10.1101/gr.244830.118

You D, Lyn-Cook LE, Gatti DM, Bell N, Mayeux PR, James LP, Mattes WB, Larson GJ, Harrill AH. 2020. Nitrosative stress and lipid homeostasis as a mechanism for zileuton hepatotoxicity and resistance in genetically sensitive mice. Toxicol Sci. 175:220–235. https://doi.org/10.1093/toxsci/kfaa037

Yu G, Li F, Qin Y, Bo X, Wu Y, Wang S. 2010. GOSemSim: an R package for measuring semantic similarity among GO terms and gene products. Bioinformatics. 26:976–978. https://doi.org/10.1093/bioinformatics/btq064

Zdraljevic S, Fox BW, Strand C, Panda O, Tenjo FJ, Brady SC, Crombie TA, Doench JG, Schroeder FC, Andersen EC. 2019. Natural variation in C. elegans arsenic toxicity is explained by differences in branched chain amino acid metabolism. Elife. 8;8:e40260. https://doi.org/10.7554/eLife.40260

Zeise L, Bois FY, Chiu WA, Hattis D, Rusyn I, Guyton KZ. 2013. Addressing human variability in next-generation human health risk assessments of environmental chemicals. Environ Health Perspect. 121:23–31. https://doi.org/10.1289/ehp.1205687

Zhang G, Roberto NM, Lee D, Hahnel SR, Andersen EC. 2022. The impact of species-wide gene expression variation on Caenorhabditis elegans complex traits. Nat Commun. 13:3462. https://doi.org/10.1038/s41467-022-31208-4

Zhou S, Luoma SE, St Armour GE, Thakkar E, Mackay TFC, Anholt RRH. 2017. A Drosophila model for toxicogenomics: genetic variation in susceptibility to heavy metal exposure. PLoS Genet. 13:e1006907. https://doi.org/10.1371/journal.pgen.1006907